International Journal of Plasticity 99 (2017) 81–101

Contents lists available at ScienceDirect

International Journal of Plasticity

journal homepage: www.elsevier.com/locate/ijplas

Effect of dislocation density-twin interactions on twin growth in AZ31 as revealed by explicit crystal plasticity finite element modeling

Milan Ardeljan [a], Irene J. Beyerlein [b], Marko Knezevic [a, *]

[a] Department of Mechanical Engineering, University of New Hampshire, Durham, NH 03824, USA
[b] Mechanical Engineering Department, Materials Department, University of California Santa Barbara, Santa Barbara, CA 93106-5070, USA

ARTICLE INFO

Article history:
Received 8 May 2017
Received in revised form 6 September 2017
Accepted 7 September 2017
Available online 15 September 2017

Keywords:
Twinning
Microstructures
Crystal plasticity
Finite elements
Dislocation density

ABSTRACT

In this work, we employ the recently developed framework for the explicit modeling of discrete twin lamellae within a three-dimensional (3D) crystal plasticity finite element (CPFE) model to examine the effects of dislocation densities in the twin domain on twin thickening. Simulations are carried out for $\{\bar{1}012\}\langle 10\bar{1}1\rangle$ extension twins in a magnesium AZ31 alloy. The model for the twin lamellae accounts for the crystallographic twin-matrix orientation relationship and characteristic twin shear transformation strain. The calculations for the mechanical fields as a result of twinning consider that one of three types of twin-dislocation density interactions have occurred. One case assumes that the expanding twin retains in its domain the same dislocation density as the parent. The second one considers that twin expansion has lowered the dislocation density as the twin thickens, and the last one, the Basinski effect, assumes that when twin sweeps the region, the dislocation density incorporated in the twin domain is amplified. In the modeling approach, the twin is thickened according to a criterion that maintains the stress state in the vicinity of the grain at a pre-defined characteristic twin resistance. The calculations show that most of the averaged properties, such as the rate of dislocation storage in the entire twin grain, the twin growth rate, the stress field in the twinned grain and neighboring grains, and the slip activity in the parent matrix are not significantly altered by dislocation storage in the twin. The results indicate that, however, the slip activity in the twinned domain is affected. In particular, in the increased dislocation density case, the rate of dislocation density in the twin domain increases at low strains when the twin is first growing from 2% to 5% volume fraction. This initial boost in the dislocation density storage rate causes the newly expanded dislocation twin to contain more stored dislocations than the other cases for all strain levels. Another interesting difference concerns the preference for one or two twins for the same total twin volume fraction; for the increased dislocation twin or twin that retains the dislocation density as it grows, formation of two twins is favored. For a twin that removes dislocation density, only one twin is preferred. The results imply that in the case with reduced dislocation density leads to lower stored dislocations and dislocation storage rates, and lower pyramidal slip activity.

* Corresponding author. University of New Hampshire, Department of Mechanical Engineering, 33 Academic Way, Kingsbury Hall, W119, Durham, NH 03824, USA.
E-mail address: marko.knezevic@unh.edu (M. Knezevic).

http://dx.doi.org/10.1016/j.ijplas.2017.09.002
0749-6419/

1. Introduction

Deformation twinning is an important deformation mechanism, governing both anisotropy and tension-compression asymmetry, as well as texture evolution of many polycrystalline metals, particularly those with low symmetry crystal structures, such as hexagonal (e.g., Mg, Ti, Zr, and its alloys) and orthorhombic (e.g., U). Understanding the effects of deformation twinning on mechanical fields within the grain, its neighbors, and overall material behavior calls for knowledge on how twinning initiates and progresses in time and throughout the grain structure.

Often deformation twinning operates along with dislocation slip as the material is mechanically deformed. How deformation twins propagate is heavily dependent on the interactions between the growing twin lamellae and gliding dislocations. Three main slip-twin interactions, which have been studied via experiment, simulation, and theory, are the volume effect, the barrier effect, and nucleation (Basinski and Basinski, 1989; Beyerlein et al., 2014; Capolungo et al., 2009; Cheng and Ghosh, 2015; El Kadiri and Oppedal, 2010; Fromm et al., 2009; Jahedi et al., 2017; Kaschner et al., 2006; Knezevic and Landry, 2015; Knezevic et al., 2013b, 2013c, 2013d; Salem et al., 2003). The first one refers to the lattice reorientation imparted by a twin. The new orientation can alter the preferred slip modes from that of the original parent. The amount of shearing associated with the twin is governed crystallographically by the characteristic twin shear. This value for extension twins in Mg is 0.1289, and thus other deformation mechanisms, such as slip, must be operating in the crystal at the same time. The second one concerns the misorientation imparted at the twin-matrix interface. The alteration in the crystallographic slip planes can pose a barrier to some gliding dislocations. The last one raises the issue of twin nucleation. It has been posed that twins form from slip dislocations (Capolungo and Beyerlein, 2008; Christian and Mahajan, 1995; Mahajan, 2013; Mendelson, 1969, 1970). The latter, in particular, suggests that dislocation glide occurs before as well as during twinning. Taken together, whether twins occur after or during dislocation glide, these issues motivate the questions: what happens to the dislocations stored in the volume of the crystal that later transforms into a twin? How would the fate of these inherited dislocations affect further growth of the twin?

These questions were first addressed by Basinski et al. based on TEM studies of copper (Basinski and Basinski, 1989; Basinski et al., 1997). The Basinski mechanism posits that an increment in strength and/or hardness develops as a result of dislocations changing from glissile parent grain to sessile configurations within twins. It is the geometrical change of dislocation Burgers vector. The mechanism was extended to HCP crystals in (Niewczas, 2010), where the details of vector transformation in those crystals are described. Many works have sought to study this dislocation-twin interaction as twins form and thicken in HCP metals. In studying the deformation behavior of unalloyed titanium at room temperature, Salem et al. (2006). revealed two competing effects of deformation twinning on the overall strain-hardening response: strain *hardening* via the Hall–Petch mechanism (i.e., a reduction in the effective slip length) and the Basinski mechanism. Micro- and nanohardness measurements revealed that deformation twins (immediately after being formed) were harder than the matrix (almost 30%), regardless of the twin thickness and orientation, thus supporting the Basinski mechanism.

El Kadiri and Oppedal (El Kadiri and Oppedal, 2010) proposed the idea of dislocation transmutation. As the parent slips and the twin grows, the twin finds an increasing density of dislocations to incorporate and transmute. The multiplicity of dislocation types in HCP metals, inherited by the twin from the parent, would suggest that the twin stores dislocations more rapidly than the parent. Due to the coherent crystallographic character of the extension twin boundary with parent grain, transmission of dislocations from parent to twin is higher than that to the parent from its neighbors. Additionally, transmutation of dislocations from parent to twin can cause dislocation rearrangements or reconfigurations that leads to dislocation generation. The effect is more pronounced due to the operation of multiple slip modes under deformation of the HCP Mg structure. As such, transmutation results in a higher fraction of dislocation types within the twinned regions than in the parent, forcing them to interact and induce an increasing latent hardening unique for twinning.

Using a 3DXRD experimental technique, capable of tracking the full stress tensor in a grain and an evolving twin, Aydiner at el (Aydıner et al., 2009). examined the formation of a twin within a parent grain during compression of an AZ31 Mg alloy with the c-axis of the parent grain nearly parallel to the compression axis. The results showed that the stress state in the newly formed twin was lower than that of the parent grain. Using a full-field discrete FFT model, Kumar et al (Arul Kumar et al., 2016). were able to explain the reduction in stress by a backstress that develops in the twin via a reaction from the neighboring crystals to the shear of twin. In this work, the effect of dislocation density in the twin or changes in this density before and after twinning was not studied.

Using 3D-XRD (Bieler et al., 2014), studied strongly textured pure Ti after 1.5 percent tensile strain to nucleate $\{10\bar{1}2\}$ twins. They show that before the twin happens, the stress state in the parent grain is lower prior to twin formation. Apparently, the twin raises the stress in the parent grain after the twin formed. As a further addition to the conclusion made by (Aydıner et al., 2009), they conclude that the deformation history in the neighboring grains also needs to be considered in understanding the stress and strain state of the twin.

Recently, we developed a framework for modeling discrete twin lamellae within a three dimensional (3D) crystal plasticity finite element (CPFE) model (Ardeljan et al., 2015b). The CPFE model accounts for the shear transformation strain and reorientation associated with deformation twinning. These calculations were carried out for twinning in uranium, which has an orthorhombic crystal structure and twins predominantly on the $\{130\}\langle 3\bar{1}0\rangle$ systems under ambient conditions. This new technique is a useful tool for studying 3D stress states generated by deformation twin lamellae.

More recently, another approach was developed for modeling discrete twin evolution in polycrystalline microstructures using crystal plasticity finite element framework (Cheng and Ghosh, 2017). The physics of twin nucleation was based on the dissociation of sessile dislocations into stable twin loops, while propagation was assumed to proceed by atoms shearing on twin planes and shuffling to reduce the thermal activation energy barrier. Explicit twinning was accomplished using the evolution of state variables instead of inserting and propagating twins as separate geometrical objects. The work facilitated modeling of many discrete twins in the microstructure without frequent remeshing. However, the applied plastic strain accommodated by the twin may not have corresponded to the twin volume.

In this work, we apply the technique from (Ardeljan et al., 2015b) to study the generation of 3D stress fields produced by the $\{\bar{1}012\}\langle 10\bar{1}1\rangle$ extension twins an Mg alloy AZ31. The constitutive law accounts for anisotropic elastic and plastic behavior and uses a hardening law based on thermally activated dislocation density evolution on three modes of slip: basal a, prismatic a, and pyramidal c + a slip. This approach is used to investigate the influence of the *twin-dislocation density interactions* and the dislocations within the new twin domain that were inherited from the crystalline region before it transformed into a twin after the twin first formed on the driving forces for further growth under mechanical loading.

With the model, we explore the effect of the dislocation density in the twin on the mechanical fields in the crystal as well as the driving forces for further twinning. When the twin is first nucleated and propagated, a twin-dislocation density is assigned point by point within the lamellae. The twin dislocation density is dictated by one of three relationships to the current stored dislocation density at that same point in the volume. The first relation considers one extreme, in which the prior dislocation density is annealed, the second one the other extreme, which is the Basinski effect, wherein the dislocation density is twice as high, and finally the last situation presumes that the dislocation density point for point is unchanged just before and after twinning. With the model, we investigate the three cases of twin thickening on dislocation density storage and their effects on the rate of dislocation storage in the entire twin grain, the twin growth rate, the stress field in the twin and neighboring grains, and the slip activity inside and outside the twin. Interestingly, many of these properties are not significantly altered by how the twin thickening interacts with stored dislocations. An important effect confirmed here by modeling is that the entire grain with the increased dislocation twin contains more stored dislocations and thus becomes harder as the applied strain is increased. It is also observed that for the same overall twin volume fraction, formation of two twins is more energetically favorable.

when the density of dislocations within the twin increases or remains constant. On the other hand, formation of a single twin is favored when the overall dislocation density within the twin decreases with applied strain. We examine how the preference for self-thickening of the twin lamella is affected by different dislocation storage rates, stored dislocations, and pyramidal slip activity.

2. Modeling framework

Fig. 1 shows a detailed schematic of the multi-level modeling framework utilized in this work. The model evaluates the material response at several length levels going from the right (finer level) to the left side (coarser level). At the coarse length

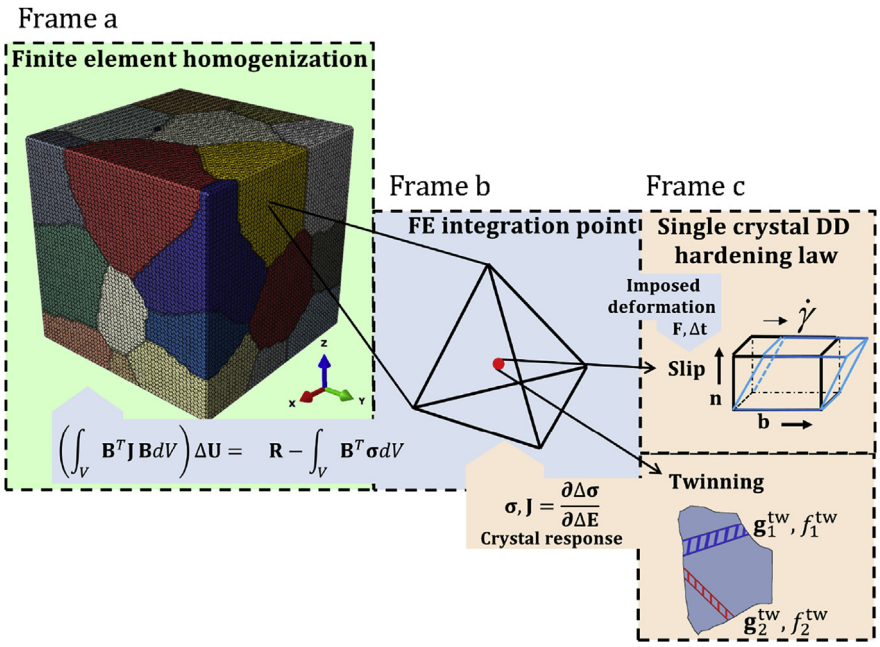

Fig. 1. Schematic of the modeling framework.

level (frame a) we have the finite element (FE) model where we have introduced the concept of grains. Each grain represents a specific element set that is composed of many finite elements with integration points (frame b). The constitutive response at each integration point is determined by the use of crystal plasticity theory which considers the underlining activity of the crystallographic slip and deformation twinning (frame c) which operate concurrently as the main mechanisms of crystal deformation. As a criterion to initiate twinning, we employ a pseudo-slip model to accumulate the strain to a critical amount (Van Houtte, 1978). Once this criterion is met, we explicitly model the twin lamella(e) by reorienting the lattice and applying the characteristic twin shear. The overall response of the granular microstructural model (polycrystal) is calculated using the finite element homogenization method which satisfies both stress equilibrium and strain compatibility conditions (in the weak numerical sense). This model provides a realistic modeling tool for capturing the effects of grain-grain interactions and heterogeneities in the stress-strain fields, all very important aspects when investing the twin-matrix composite.

Other models have been developed for the explicit modeling of a twin lamella in a microstructural framework (Knezevic et al., 2016b; Kumar et al., 2015; Zhang et al., 2008). In these works, the stress fields that develop under relatively small strain levels were studied and hardening was not as critical. In this work, the applied strains will reach moderate levels and the local stresses and strains can grow to be intense. For this reason, the constitutive response employed here includes a hardening law and permits local lattice rotations.

The constitutive equations that govern material response are numerically implemented in the User MATerial (UMAT) subroutine and executed in Abaqus Standard. The applied load, prescribed by the appropriate boundary conditions is discretized into increments, where the global stress equilibrium solution is achieved for each and every of the time increents in an iterative way using the FE method. The finite element governing equation, in its linearized form, that secures stress equilibrium and strain compatibility for each finite element is:

$$\left(\int_V \mathbf{B}^T \mathbf{J} \mathbf{B} dV\right) \Delta \mathbf{U} = \mathbf{R} - \int_V \mathbf{B}^T \boldsymbol{\sigma} dV. \tag{1}$$

In this relationship, on the left hand side $\mathbf{B}$ stands for FE strain-displacement matrix, $\mathbf{J}$ is material Jacobian matrix, $\Delta\mathbf{U}$ is displacement increment solution, while on the right hand side $\mathbf{R}$ represents the applied force vector and $\boldsymbol{\sigma}$ is the Cauchy stress tensor (Bathe, 1996).

Below we summarize the constitutive formulation that relates the stress to the strain work conjugate applied at each integration point within each element in the finite mesh (Ardeljan et al., 2014; Kalidindi et al., 1992, 2006; Knezevic et al., 2014d; Savage et al., 2017a; Savage et al., 2017b; Zecevic and Knezevic, 2017; Zecevic et al., 2015b, c). The following notation is used: tensors are denoted using boldface symbols, which are not italic and scalars are denoted using italicized symbols, which are not bold.

2.1. Kinematics of slip and twinning within CPFE

In the description that follows, the main kinematic variables of velocity gradient and deformation gradient are denoted by $\mathbf{L}$ and $\mathbf{F}$, respectively. $\mathbf{L}$ is the sum of the elastic $\mathbf{L}^e$ and plastic $\mathbf{L}^p$ velocity gradients

$$\mathbf{L} = \mathbf{L}^e + \mathbf{L}^p. \tag{2}$$

The $\mathbf{L}^p$ is the sum of the contributions from slip and twinning as follows

$$\mathbf{L}^p = \mathbf{L}^{sl} + \mathbf{L}^{tw}. \tag{3}$$

The velocity gradients for slip and twinning, are given by:

$$\mathbf{L}^{sl} = \sum_{\alpha}^{N^{sl}} \dot{\gamma}^{\alpha} \mathbf{m}_0^{\alpha}, \quad \mathbf{L}^{tw} = \sum_{\beta}^{N^{tw}} f^{\beta} S^{\beta} \mathbf{m}_0^{\beta}, \tag{4}$$

where $\dot{\gamma}^{\alpha}$ is the shear rate on slip system α, $\mathbf{m}_0^{\alpha}$ and $\mathbf{m}_0^{\beta}$ are the Schmid tensors for slip system α and twin system β, respectively, S^{β} is the characteristic twin shear, and N^{sl} and N^{tw} are the total number of available slip and twin systems, respectively. The Schmid tensors are defined as the dyadic product of two orthogonal unit vectors denoting the slip (or twin) shear direction and the slip (or twin) plane normal, respectively. The subscript '*0*' denotes that these tensors are known *a priori* and use the initial crystal orientation.

The evolution equation for the twin volume fraction of a given slip system β is given by:

$$\dot{f}^{\beta} = \frac{\dot{\gamma}^{\beta}}{S^{\beta}}, \tag{5}$$

or in strain increment form, $\Delta f^{\beta} = \frac{\Delta\gamma^{\beta}}{S^{\beta}}$ (Kalidindi, 1998; Van Houtte, 1978). The complete twin shear strain of 0.1289 is obtained when the volume fraction of a particular extension twin system, β, reaches unity, i.e., $\sum_1^n \Delta f^{\beta} = 1$, for a certain number of n strain increments, and as a result, $S^{\beta} = \sum_1^n \Delta\gamma^{\beta}$.

The total deformation gradient tensor ($\mathbf{F}$) for finite deformations can be decomposed into its elastic and plastic components via:

$$\mathbf{F} = \mathbf{F}^e\mathbf{F}^p, \tag{6}$$

where $\mathbf{F}^e$ contains deformation gradients associated with both elastic stretching and lattice rotation, while $\mathbf{F}^p$ is the deformation gradient due to plastic deformation alone. The following flow rule relationship is used to define the evolution of $\mathbf{F}^p$ in a rate form:

$$\dot{\mathbf{F}}^p = \mathbf{L}^p\mathbf{F}^p, \ \frac{d\mathbf{F}^p}{dt} = \mathbf{L}^p\mathbf{F}^p. \tag{7}$$

Integrating Eq. (7) from t to $\tau = t + \Delta t$, gives

$$\mathbf{F}^p(\tau) = exp(\mathbf{L}^p\Delta t)\mathbf{F}^p(t). \tag{8}$$

Expressing the exponential as a series and retaining the first order terms yields

$$\mathbf{F}^p(\tau) = \{\mathbf{I} + \Delta t\mathbf{L}^p\}\mathbf{F}^p(t) = \left\{\mathbf{I} + \Delta t\left(\mathbf{L}^{sl} + \mathbf{L}^{tw}\right)\right\}\mathbf{F}^p(t), \tag{9}$$

where $\mathbf{I}$ is the identity matrix. The constitutive equation for the stress in the grain is given by

$$\mathbf{T}^e = \mathbf{C}\mathbf{E}^e, \ \mathbf{T}^e = \mathbf{F}^{e^{-1}}\{(det\mathbf{F}^e)\boldsymbol{\sigma}\}\mathbf{F}^{e^{-T}}, \ \mathbf{E}^e = \frac{1}{2}\left\{\mathbf{F}^{e^T}\mathbf{F}^e - \mathbf{I}\right\}, \tag{10}$$

where $\mathbf{C}$ is the fourth-order elasticity tensor (Landry and Knezevic, 2015; Wu et al., 2007), $\mathbf{T}^e$ and $\mathbf{E}^e$ are a pair of work conjugate stress and strain measures, and $\boldsymbol{\sigma}$ is the Cauchy stress for the grain. The elastic deformation gradient $\mathbf{F}^e = \mathbf{F}\mathbf{F}^{p^{-1}}$ is determined by first rewriting Eq. (9) as:

$$\mathbf{F}^{p^{-1}}(\tau) = \mathbf{F}^{p^{-1}}(t)\left\{\mathbf{I} - \Delta t\left(\mathbf{L}^{sl} + \mathbf{L}^{tw}\right)\right\}. \tag{11}$$

The $\mathbf{L}^{tw}$ is conveniently divided into two parts, $\mathbf{L}^{tw,\,pts}$ and $\mathbf{L}^{tw,ots}$, i.e.,

$$\mathbf{L}^{tw} = \mathbf{L}^{tw,pts} + \mathbf{L}^{tw,ots}. \tag{12}$$

where $\mathbf{L}^{tw,\,pts}$ is the velocity gradient of the most active variant, or the so-called predominant twin system (*pts*) and $\mathbf{L}^{tw,\,ots}$ is the velocity gradient contributed by the other twin systems. Note that every twin system is active in every grain of the polycrystal throughout a plastic deformation process, while continuously accumulating twin volume fraction with plastic strain based on the pseudo-slip model (Van Houtte, 1978). Once the value of accumulated twin volume fraction of a specific twin system (*pts*) reaches a prescribed threshold value to nucleate or thicken within a given grain, the criterion is met to explicitly propagate or thicken the twin lamella by reorienting the lattice with respect to parent grain and enforcing the characteristic twin transformation shear.

2.2. Kinetics of slip and twinning

To determine the shear strain rate $\dot{\gamma}^{\alpha}$, for each slip system α, and $\dot{\gamma}^{\beta}$, twinning systems β, we use a relationship between the resolved shear stress ($\tau^{\alpha} = \mathbf{T}^e\cdot\mathbf{m}_0^{\alpha}$ for slip and $\tau^{\beta} = \mathbf{T}^e\cdot\mathbf{m}_0^{\beta}$ for twinning, where '$\cdot$' represents the dot product) with their characteristic resistance (τ_c^{α} for slip systems and τ_c^{β} for twin systems) following a power-law relationship given by (Asaro and Needleman, 1985; Hutchinson, 1976; Kalidindi, 1998):

$$\dot{\gamma}^{\alpha}=\dot{\gamma}_0\left(\frac{|\tau^{\alpha}|}{\tau_c^{\alpha}}\right)^{\frac{1}{m}}sign(\tau^{\alpha}),\ \dot{\gamma}^{\beta}=\begin{cases}\dot{\gamma}_0\left(\frac{\left|\tau^{\beta}\right|}{\tau_c^{\beta}}\right)^{\frac{1}{m}}sign\left(\tau^{\beta}\right) & if\ \tau^{\beta}>0\\ 0 & if\ \tau^{\beta}<0\end{cases}, \tag{13}$$

where $\dot{\gamma}_0$ is a reference slip rate (arbitrarily set to be 0.001 s^{-1}) and m is a strain rate sensitivity factor (set to be 0.02 for both slip and twinning systems).

For the τ_c^{α} and τ_c^{β} evolution, we use the hardening law for AZ31 described in (Ardeljan et al., 2016). The hardening law adopted is a dislocation density based hardening law employing rate equations for dislocation density including thermally activated dynamic recovery. The basic formulation of this particular hardening law dates back to 2008 (Beyerlein and Tomé, 2008) and since then has been adapted for simulation of several low symmetry metal systems including Be (Knezevic et al., 2013a; Zecevic et al., 2015a), Zr (Knezevic et al., 2015b; Zecevic et al., 2016a), Mg (Lentz et al., 2015a, 2015b; Risse et al., 2017), Ti (Zecevic et al., 2017), and U (Knezevic et al., 2012, 2016a; Zecevic et al., 2016b, c) as well as cubic metals (Knezevic et al., 2014a, 2014b, 2015a; Zecevic and Knezevic, 2015; Zecevic et al., 2016d). The equations are provided in appendix A, while the parameters for AZ31 used in this work are taken from (Ardeljan et al., 2016).

3. Explicit incorporation of twinning in CPFE

3.1. Starting 3D microstructures

We produced a synthetic microstructure using the publicly available software called DREAM.3D, which stands for Digital Representation Environment for the Analysis of Materials in 3D (Groeber et al., 2008; Groeber and Jackson, 2014). Compared to those typically generated via the Voronoi tessellation scheme, DREAM.3D generates grain morphology and grain size distribution that are more realistic. DREAM.3D provides 3D synthetic voxel-based microstructures and surface meshes for each individual grain based on specified grain size and grain shape distributions. For our interests, we further define voxel density/resolution in the model in order to achieve the desired number of surface finite elements. We use the surface mesh as a bridge between a voxel-based model and a volumetric (in our case tetrahedral) mesh.

The surface mesh is used for 3D mesh generation. Starting from the surface mesh, 3D solid meshing of individual grains is performed to ensure 'conformal' grain boundaries in MSC Patran Version (2013). Conformal boundaries mean mesh conformance between grain boundaries, an aspect that is important when phenomena due to grain-to-grain interactions need to be analyzed, such as stress concentrations at quadruple points. The reader can find a detailed step-by-step explanation of this meshing procedure in (Knezevic et al., 2014c).

3.2. Procedure of incorporating and thickening of twin lamellae in an FE mesh

Explicitly including a twin lamella into the finite element framework required the development of an automated procedure. Hence, scripting capabilities offered in software packages such as Matlab, Patran and Abaqus were successfully employed. This procedure is described in detail in (Ardeljan et al., 2015a; Ardeljan et al.) and consists of several geometric manipulations and mesh generations. For this purpose, we developed a script in Matlab, which writes Patran and Python script files containing specific commands for Patran and Abaqus, respectively. The Patran scripts perform either surface or solid meshing and the Python script files either extract the surface mesh from the solid mesh model or perform the Abaqus mesh cleanup procedure. After this procedure is initially performed in this study, the final result is a twin lamella with a 2% volume fraction inserted with the appropriate crystallographic orientation and shape relative to a selected parent grain that maintains the overall conformity with the parent and neighboring grains. Further executions of this procedure result in thickening of a priory nucleated and propagated twin lamella according to prescribed twin volume fraction values.

3.3. Procedure for enforcing the characteristic twin shear within reoriented twin lamella volume

So far, we explained all the necessary geometric and FE mesh operations in order to form and thicken the twin lamella. However, to fully model the twin, in addition to the crystal lattice reorientation, intrinsic shearing imposed by creating and thickening twin lamella must be kinematicaly consistent (Ardeljan et al., 2015b). Once the twin lamella is formed, the volume fraction of the predominant twin system ($\beta = tw, pts$) in the corresponding volume reaches unity. To ensure that the strain accommodated by the twin variant $\beta = tw, pts$ corresponds to its volume transferred from the parent either during the twin formation or subsequent thickening, we enforce the twinning shear strain in the twin using

$$\mathbf{F}^{p^{-1}}(\tau)=\left\{\mathbf{I}-S^{tw,pts}\mathbf{m}_0^{tw,pts}\right\}. \tag{14}$$

Additionally, we ensure that any strain accommodated by the same selected twin variant is removed from the parent grain using

$$\mathbf{F}^{p^{-1}}(\tau) = \mathbf{F}^{p^{-1}}(t)\left\{\mathbf{I} + f^{tw,pts} S^{tw,pts} \mathbf{m}_0^{tw,pts}\right\}. \tag{15}$$

In the above equations, $f^{tw,pts}$ is the accumulated volume fraction of the selected twin variant in the parent grain. Both Eqs.((14) and (15) follow from Eq. (11) and take into account Eq. (5). In summary, Eqs. (14) and (15) enable the required transfer of strain after a twin has formed from the parent to the twin by updating values of $\mathbf{F}^p$ which is simultaneously carried out for all elements belonging to the parent grain and twin.

4. AZ31 twin model

4.1. The model set up

Fig. 2 shows the 3D FE microstructural model. This 3D microstructure contains 29 grains and approximately 570,000 finite elements. Each grain consists of roughly 20,000 finite elements. Discretization uses linear tetrahedral elements with one integration point (i.e., type C3D4 in ABAQUS). In order to reveal the interior of the model and to show the grain morphologies, we cut the model in half and expose the two cut planes (see the two right-most images in Fig. 2).

We randomly assign crystal orientations to every grain except the green grain in the center of the FE model. The crystal orientation of this grain is selected such that it favors $\left\{\bar{1}012\right\}\left\langle 10\bar{1}1\right\rangle$ extension twinning under simple compression along the normal direction (ND), i.e. z-direction (Fig. 3). The simple compression is performed by imposing displacement in the z-direction (ND), where the lateral sides are traction-free, and hence free to expand. The compression consists of several deformation steps, necessary to initially form and then thicken the twin lamella, as will be detailed below. The chosen parent grain orientation is defined by Bunge-Euler angles of $(50^\circ, 95^\circ, 180^\circ)$. The same crystal orientation is assigned to each finite element within each grain, which results in the initial intra-granular misorientations of zero for each grain. Supplementary material of the paper contains the model setup.

For the 3D model grain structure and central grain, once a threshold is reached for twin nucleation, it needs to be inserted, and where it is inserted in the microstructure could have a significant influence on its subsequent growth characteristics. Thus, the key question is where should it form? Twins are a localized phenomenon and not strongly correlated with average properties or average stresses or strains (Christian and Mahajan, 1995). Twins are most likely to form at points with the highest stress concentration (Bell and Cahn, 1957; Wang et al., 2010a). For the stress concentration component, we elect to use, as a driving force, the resolved shear stress on the twin plane and in the twinning direction (RSSTW) and calculate the stress concentration in RSSTW by considering the value of RSSTW normalized by its critical value, which evolves with deformation and it is governed by dislocation density hardening law. Before moving forward, it is important to keep in mind that the full tensorial fields are calculated at every increment. Should another driving force be deemed more appropriate, it can be easily calculated and used.

Prior to the initial twin lamella formation, a pre-strain of approximately 0.002 in simple compression was applied to a polycrystal along the z-direction. As an implication of a local stress-driven event, it is not necessary that the twin variant with the highest Schmid factor based on the average grain orientation and the applied compression ND load would be the variant that would form. For the purpose of the extension twin variant selection and determining where to insert the twin lamella,

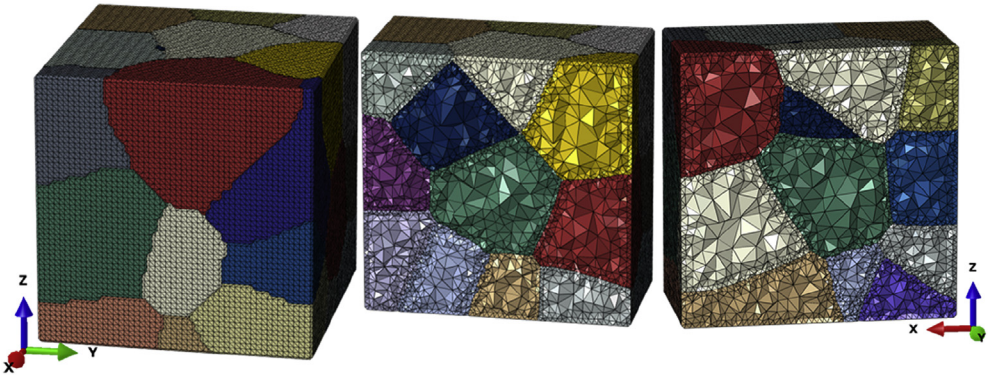

Fig. 2. A finite element model of explicit grain structure that consists of 29 grains and 570,000 C3D4 elements. The two semi-sections that are perpendicular to each other show the interior of the granular model where the initial crystal orientation of the central grain (colored in green) is set to be favorable for $\left\{\bar{1}012\right\}\left\langle 10\bar{1}1\right\rangle$ extension twinning for simple compression along the z-direction (ND direction). Note that the models on the left and in the middle are in one, while the model on the right is in a different frame. (For interpretation of the references to colour in this figure legend, the reader is referred to the web version of this article.)

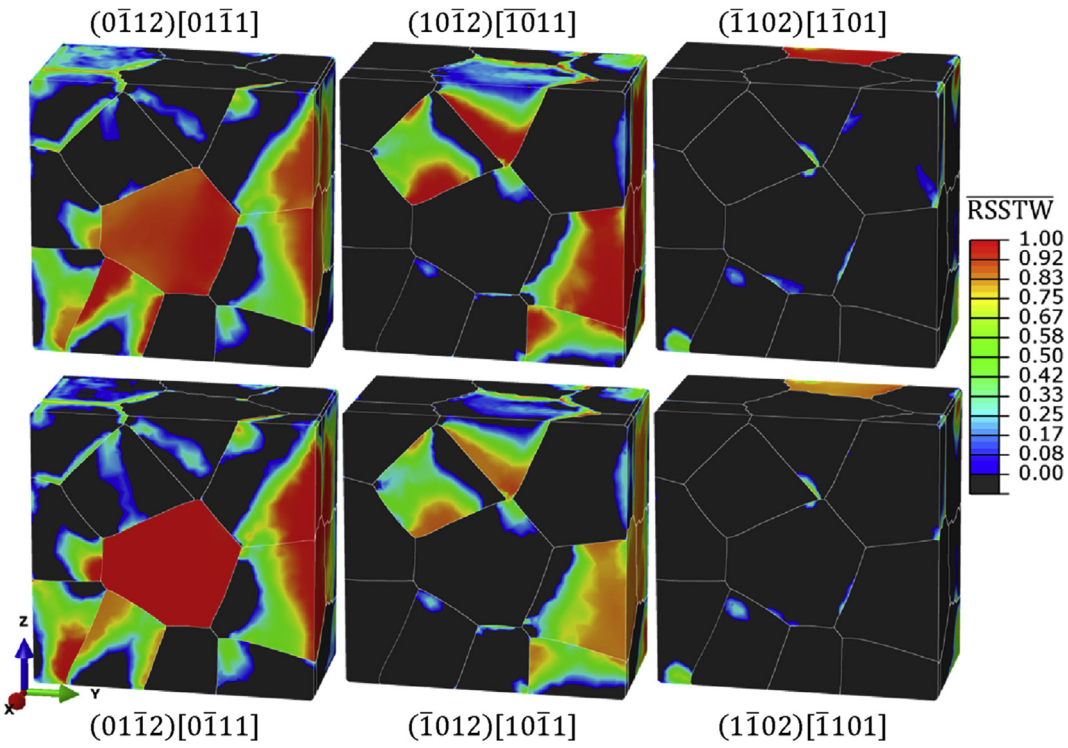

Fig. 3. Distributions of normalized resolved shear stresses ($\overline{\text{RSSTW}}$) along the twin plane in the twin direction for all six extension variants after a pre-strain of approximately 0.002 necessary to nucleate initial twin lamella. Normalization was performed with corresponding threshold values for twinning.

we study the RSSTW fields for each of the six extension variants in the grain cluster (Fig. 3). Looking at the central grain alone, we observe that two of the six variants appear to have high RSSTW values with the $(01\bar{1}2)[0\bar{1}11]$ variant being the highest and thus we choose to nucleate this variant in the simulations hereinafter. This particular extension twin variant becomes the predominant twin system (*pts*) as soon as its accumulated twin volume fraction reached a threshold value to form an initial twin lamella. In the present study, the threshold value of 2% is chosen as appropriate. Smaller than 2% is possible to handle by the procedure but is much more challenging to handle as far as geometry and mesh generation due to very small thickness.

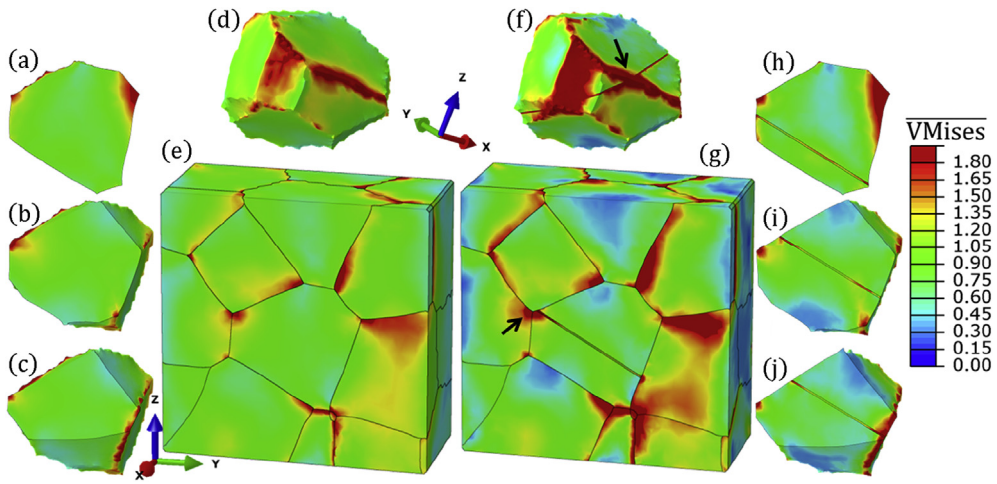

Fig. 4. Distributions of the von Mises stress normalized by the applied stress over the parent grain without a twin lamella (a–e) and after formation of 2% twin lamella (f–j). Different Y-Z sections of the parent grain at constant X are shown to expose different stress concentration points (without the twin lamella (a–c) and with 2% twin lamella (h–j)). Note that (a) and (h), (b) and (i), and (c) and (j) are the same sections at constant X with each belonging to different strain/time point (i.e. before and after the twin is propagated). Note also that grains shown in (d) and (f) are in a different frame. The black arrow indicates the location of the highest stress concentration.

Due to the specific nature of deformation in AZ31, we see that the neighboring grains could easily deform by twinning as well, but here for simplicity, we carry out explicit modeling of twin lamella for the central grain only. Note that twinning is allowed in all surrounding grains by employing the pseudo-slip model. Next, the location for the twin lamella of twin variant is determined. As mentioned earlier, it is assumed that favorable twin nucleation sites are found at the grain boundaries at points of highest stress concentration (Bell and Cahn, 1957; Beyerlein et al., 2011; Molnár et al., 2012; Wang et al., 2014, 2010b, 2010c; Zheng et al., 2012). As a measure of determining these stress concentration points we use the von Mises stress values normalized by the applied stress over the entire volume of the grain model (Fig. 4). Fig. 4(a–e) show the contours of normalized von Mises stress values after the pre-strain is applied, while (f-j) show those after the twin propagation. The point of highest stress concentration at the grain boundary of the central grain is indicated by the black arrow. The twin plane location is chosen such that it intersects the volume in the parent grain with the highest twin driving force ($\overline{\mathrm{RSSTW}}$) while also connecting the points of the highest stress concentrations found at the parent grain boundaries. Consequently, the exact location will depend not only on the properties of the parent grain, but also on neighborhood orientation and morphology and the applied strain state. Fig. 4 also shows contours of normalized von Mises stress values when 2% twin lamella is formed and very small amount of strain is applied (f-j) necessary to establish the stress equilibrium after the twin is inserted. Images show the actual location where the initial twin lamella has been placed. Images (a-c) show different Y-Z sections at constant X of the parent grain before the twin is formed, while (h-j) are the corresponding images after twin lamella is formed. We note that the assumption that twin nucleated at the point of highest stress is not necessarily always the case. The twin partial at the tip near the grain boundary and other slip transfer mechanisms across grain boundaries as well as twin transmission from grain-to-grain have also been identified as nucleation sites (Wang et al., 2010c).

After forming the twin a choice can be made about the twin dislocation density. Three extreme cases are considered. One involves fully recovering the dislocations within the transforming parent material volume in the twin. Thus the twin-dislocation density is independent of the history of the parent crystal and the strain of twin formation. In the second case, the twin-dislocation density adopts the stored dislocation density at the time of twin formation. In this case, the deformation conditions at the time the twin is first formed affect the twin-dislocation density. The last case models the Basinski effect, wherein the twin dislocation density is higher than the dislocation density stored in the crystal right before twinning.

To augment the dislocation densities while propagating and thickening the twin, the dislocation densities at the integration points associated with the mesh of the parent are transferred to the integration points corresponding to the mesh of the twin. Only the values in the parent grain located where the new mesh of the twin region exists are altered. In first case, the density in the twin volume increment corresponds to an annealed state (10^{12} m^{-2}), while the existing twin volume maintains the current heterogeneous dislocation density distribution. The new increment in volume has a homogeneous distribution of dislocation density. In the second and third cases, the dislocation densities can vary from point to point in the increment because the values are based on the current dislocation distribution in the parent transforming to the twin. These assignments to incremental volumes only set the initial dislocation density and with further straining the dislocation density in the twin is allowed to evolve. Appendix B is provided to further clarify the procedure.

4.2. The twinned grain

We first consider effect of a newly formed twin on the stress field of a deformed polycrystal. The new stress field after the twin lamella forms would influence how and where twin growth would initiate. Unless stated otherwise, the instantaneous dislocation density just before twinning is used for the twin-dislocation density. Fig. 4 compares the von Mises stress field before and after twinning. We see that the parent stress field in this cross section has not changed substantially and the largest changes occur at the twin tips, where the stress concentrations increase (Fig. 4g). Further, despite the relatively small 2% volume fraction of this newly formed twin, the stress fields in the neighboring grains have been altered. In particular, we see that relaxation occurs primarily in the neighboring grains that do not intersect the twin. Based on these results, it would seem that the same twin would thicken rather than nucleating a new twin since stress fields along the twin boundary have not dropped or decreased.

To thicken the twin from the initial 2% twin volume fraction, we apply more ND compression to the 3D grain cluster model. The twin is then made to expand in five different deformation steps to volume fractions of 5%, 10%, 20%, 36% and 45%. For the growth step, the FE mesh is altered in a similar manner as twin propagation. Maintaining the same twin normal and location of the initially propagated twin, we cut the surface mesh of the parent grain by two parallel planes with a specified separation in order to expand the twin volume (Fig. 5). In this case, the surface mesh of the parent grain is now reduced for the volume of the previously formed twin lamella. The distance between the cutting planes is changed in order to reflect the twin growth. Appendix B summarizes the procedure. Every time the twin variant propagates, the iterations are performed to ensure that the shear strain accommodated by the twin variant corresponds to its size (Eq. (14)) and that the parent grain is free of any strain accommodated by the same twin variant (Eq. (15)). In the current modeling approach of explicit twin lamellae, it is not practical to grow its volume every strain increment as the twin accommodates the plastic strain since this would be extremely computationally challenging. We chose the discrete values of twin volume fractions (e.g. 5%, 10%, 20%, 36% and 45%) to facilitate growth of the lamella to a size often observed in AZ31. The sizes of these steps were optimized by considering the distributions of normalized resolved shear stresses (Fig. 9), which is a measure of the driving force to grow a twin. The steps were not made excessively large to influence the parent's grain propensity to further twin, while they are not too small to

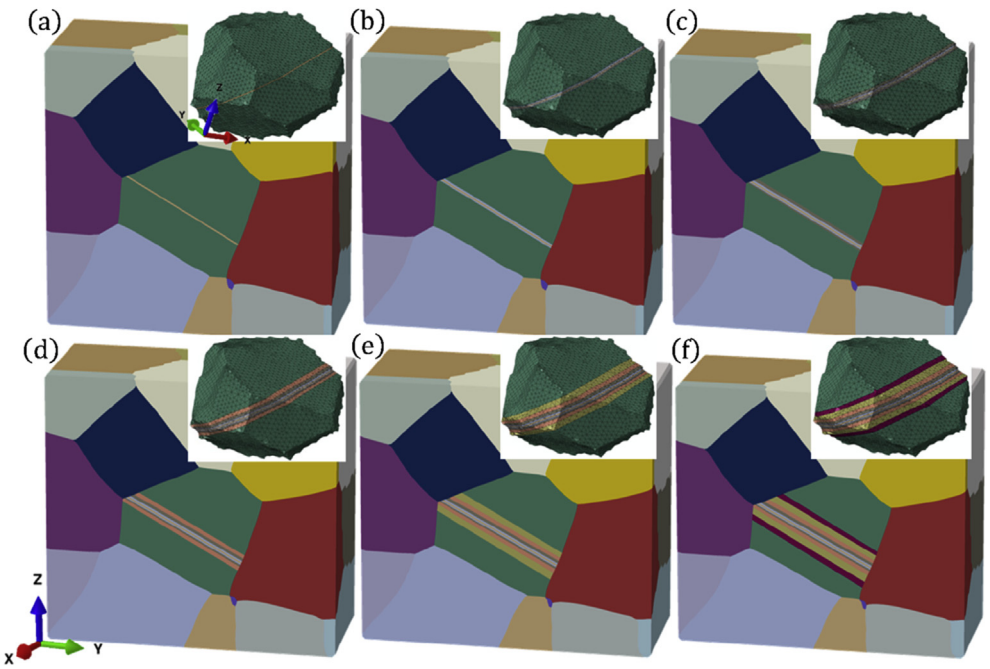

Fig. 5. Twin propagation and thickening with respect to the surrounding neighboring grains in the 3D model. Grain structure with propagated (a) 2% twin, thickened (b) 5% twin, (c) 10% twin, (d) 20% twin, (e) 36% twin and (f) 45% twin. Different colors are used to highlight the twin thickening increments. (For interpretation of the references to colour in this figure legend, the reader is referred to the web version of this article.)

unnecessary increase the deformation steps needed to achieve the target volume fraction (i.e. 45%). We ensured that more frequent increments would not reveal any new phenomena that we did not reveal with the present choices.

One of the main questions we seek to address concerns the role of the internal twin dislocation density on twin thickening. All calculations below are, therefore, repeated in the case where the dislocation density at integration points associated with the mesh are maintained before twinning (case 1, "the same dislocation twin"), or are reduced to $1 \times 10^{12}/m^2$ (case 2, "removed dislocation") or doubled from their current value before twinning (case 3, "the increased dislocation twin"). In prior work (Ardeljan et al., 2015b) the twin-dislocation density was arbitrarily assumed to adopt the current value of the stored dislocation density in the parent at the time of twin propagation and thickening (case 1, same dislocation twin).

Fig. 6 compares the von Mises stress fields produced by the twin under load. Since the hardening parameters are adjusted for AZ31, the magnitudes are realistic and thus not normalized. The stresses grow in extent and intensity as the twin grows and the applied strain increases. Many of these details are a consequence of the history of loading, the grain orientations, and the topology of the grain boundary surfaces. With all else being fixed, the comparison shows that the twin volume fraction has the greatest effect on the characteristics of the field, and comparatively, the three twin-dislocation density (DD) situations have relatively small effects. Appendix C shows von Mises contours for the other two cases (i.e. case 2 and case 3). The important point to note is that when the twin dislocation density is removed as it grows, it produces less intense regions of stress. The effect becomes more pronounced as the twin thickens. Thus, whether the twin stores additional dislocations, maintains them, or removes them as it grows, can affect localized stress states not only in the parent grain and the neighboring grain, but the next nearest neighboring grains as well.

To thicken the twin, the applied strain is increased, just enough to increase the local stress at the twin/grain boundary junction to rise again. Table 1 presents the twin volume fraction and its corresponding applied strain. As the applied strain increases to 1% and ultimately to 7.5% true strain, the twin in this particular grain thickened from its starting 2%–45% twin volume fraction.

Fig. 7 examines the rate of growth with plastic strain. The case wherein the twin removes dislocation density (DD) grows at a slightly higher rate than the other cases. Once again, the effect of the twin-DD interactions is slight, even when the twin encompasses 45% volume fraction. Fig. 8 shows the corresponding total DD (including forest and substructure) development within the twin. When the twin is just 2% volume fraction, the increased dislocation twin increases the rate of dislocation density storage over the other cases. When the twin grows larger than 2%, the effect of twin-DD interactions is negligible. However, as a consequence of the initial boost in storage rate, the accumulated DD in the entire grain is greater in the increased dislocation twin than the "same dislocation twin" or the "removed dislocation twin".

The RSSTW stress fields after the twin has thickened at every step are shown in Fig. 9. In every case the RSSTW driving stresses for the same twin system have dropped for regions within the twin lamella, which can be expected since the significant ~86° reorientation has caused other slip systems to be favored.

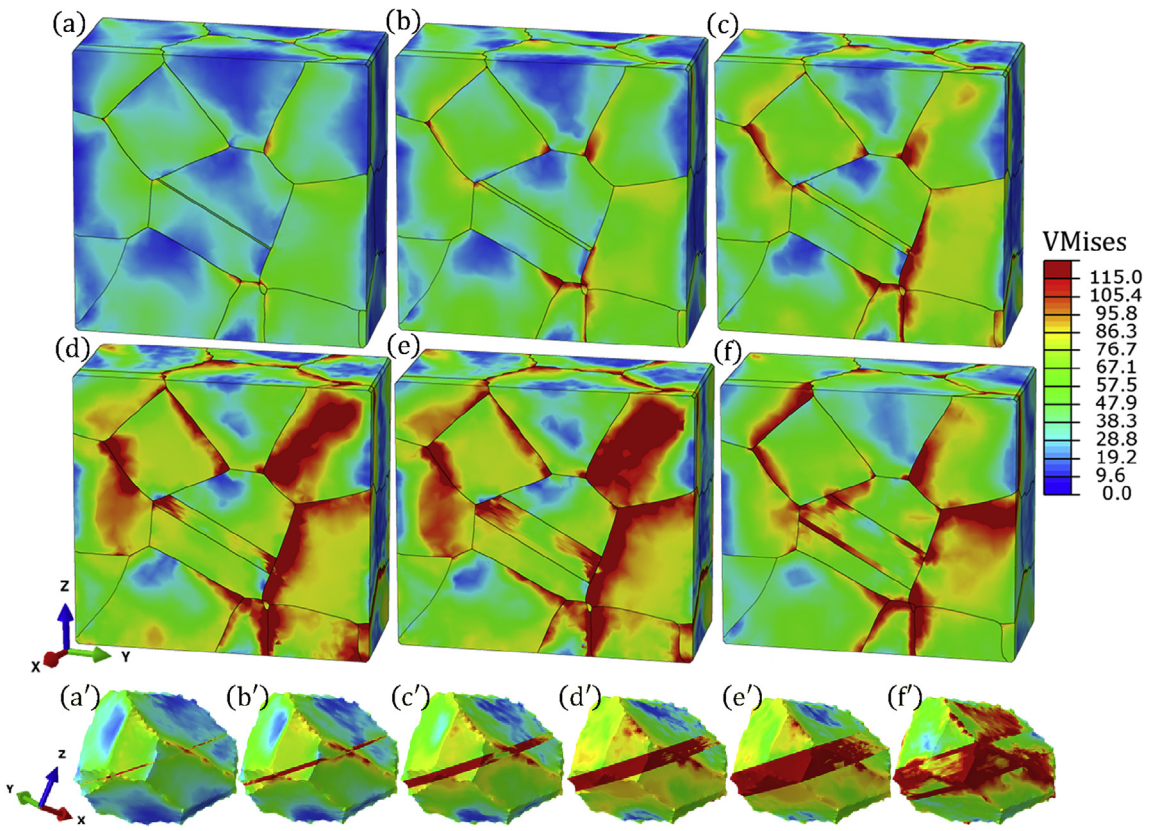

Fig. 6. Distributions of the von Mises stress (VMises) for different twin volume fractions (same dislocation twin i.e. case 1): (a and a') 2% twin, (b and b') 5% twin, (c and c') 10% twin, (d and d') 20% twin, (e and e') 36% twin and (f and f') 45% twin. In the bottom row (denoted with primed labels) the corresponding parent and twin grains pulled out from the rest of the grains in the cluster are shown.

Table 1
Different aspects of the granular structure relevant to the twin lamella formation and thickening at particular stages of this process.

TVF relative to the parent grain x10^{-2}	2.08	4.91	10.07	19.76	35.77	44.94
TVF relative to the entire FE model x10^{-2}	0.0969	0.26	0.56	1.06	2	2.44
Applied effective strain	0.0021	0.006	0.0127	0.0259	0.0489	0.0671
Effective strain accommodated by the twin	0.0019	0.0057	0.0121	0.0241	0.0434	0.0558

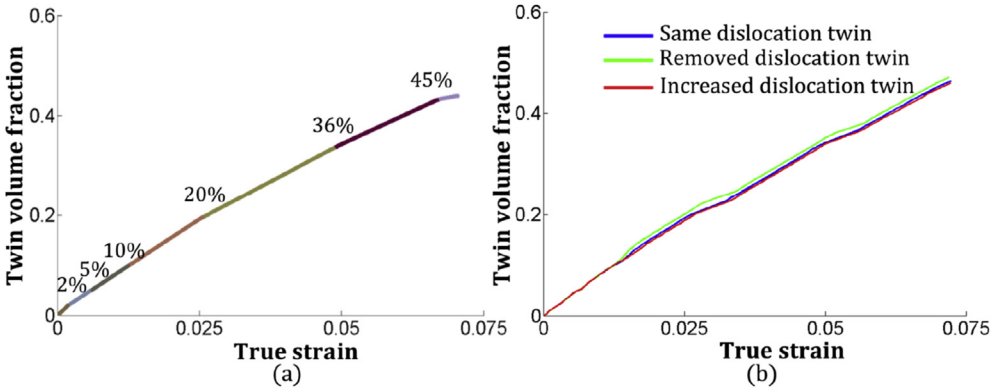

Fig. 7. Evolution of the twin volume fraction (extension twin) within the central parent grain during simple compression when (a) dislocation densities are transferred from parent to twin region "as is" (same dislocation twin) and (b) the comparison between the three cases with different dislocation density content within the twin region. In the plot 7a different colors are used for different stages (deformation steps) in the process of twin thickening. (For interpretation of the references to colour in this figure legend, the reader is referred to the web version of this article.)

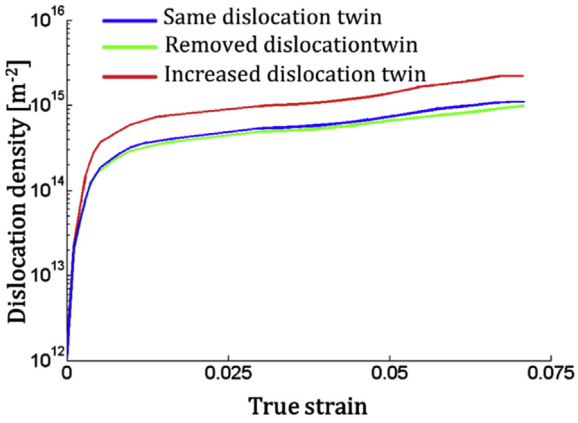

Fig. 8. Calculated dislocation density in the twin region for three considered dislocation density cases. The results for the total dislocation density in the twinned grain containing two twins are very similar.

Fig. 9 can also be used to assess the driving forces for further growth that prevail in the parent grain outside of the lamella. For a more quantitative assessment, we averaged the RSSTW on both twin planes for each twin thickness after transformation. To be more precise, this quantity of averaged RSSTW (normalized twin driving force) was calculated as $\frac{1}{V}\sum_{i=1}^{N_{el}} \frac{\tau^{tw,pts^i}}{\tau_c^{tw,pts^i}} V^i$ for a prescribed volume of the parent grain, where *tw,pts* is already defined as the predominant twin system. Fig. 10a shows the variation with twin growth in this averaged RSSTW near the twin boundary in the parent. As the twin thickens, the average RSSTW remains close to the CRSS. This serves as validation for the growth criterion and shows that the applied strain was increased just enough to thicken the twin in each case. A similar calculation of the averaged RSSTW is made for the entire matrix volume and the results are shown in Fig. 10b. In this case, the value begins to decrease as the twin thickens, suggesting that as the twin thickens at the later stages of deformation, more strain would be needed to create a new twin elsewhere and self-thickening becomes increasingly preferred.

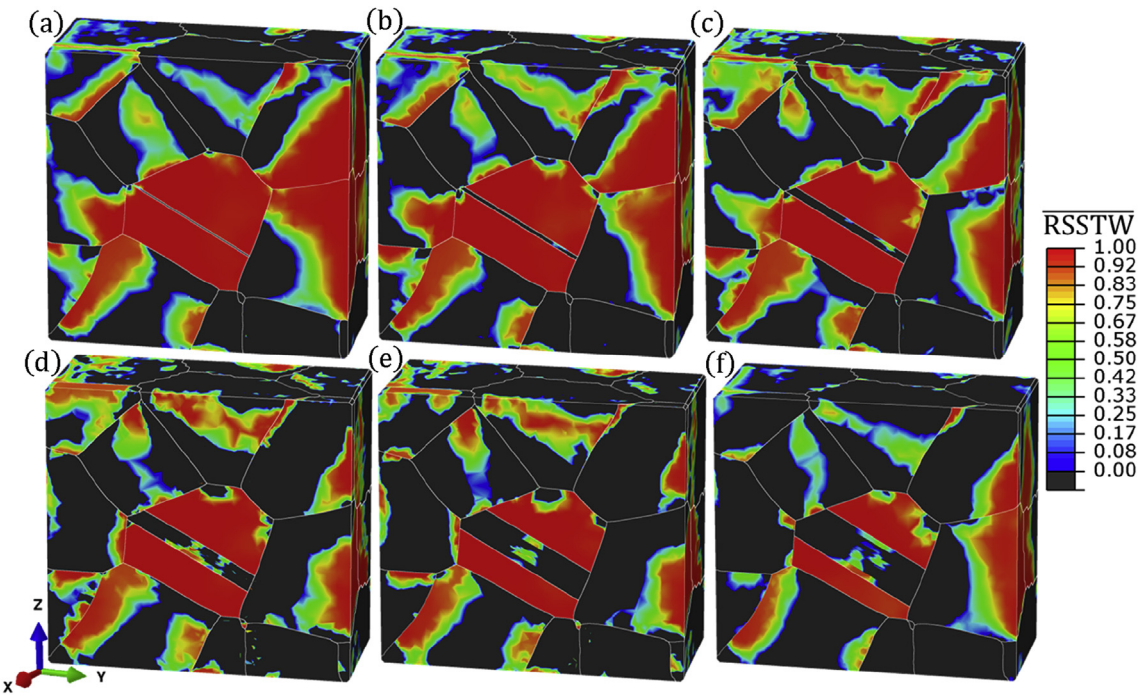

Fig. 9. Distributions of normalized resolved shear stresses along the most dominant twin plane in the twin direction ($(01\bar{1}2)[0\bar{1}11]$) for different twin volume fractions before transformation: (a) 2% twin, (b) 5% twin, (c) 10% twin, (d) 20% twin, (e) 36% twin and (f) 45% twin.

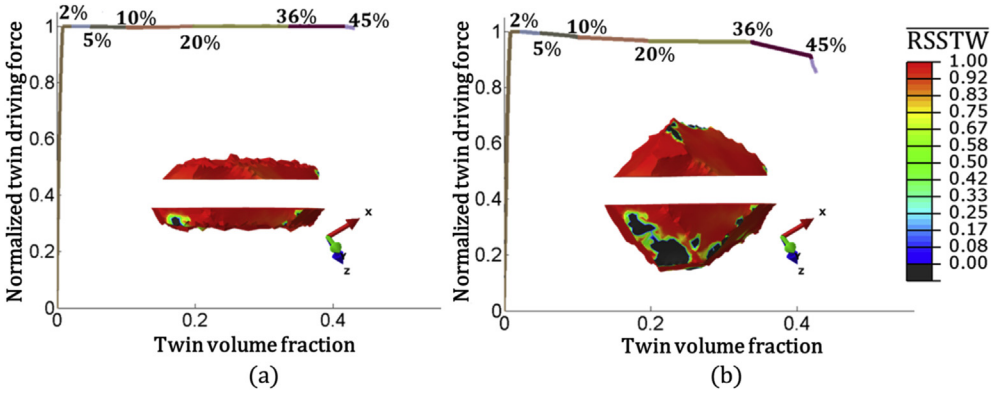

Fig. 10. Normalized twin driving force in the central parent grain calculated for different twin volume fractions using two domains: (a) volume close to twin-matrix interface and (b) the entire parent grain. Different colors are used for different stages (deformation steps) in the process of twin thickening. (For interpretation of the references to colour in this figure legend, the reader is referred to the web version of this article.)

4.3. Self-thickening versus two twins

In the above simulations, the increase in applied work is dissipated by the increase in twin thickness, since the average driving force along the twin plane surfaces is maintained just at the characteristic stress for twinning. We find that the driving force is also maintained in the remainder of the parent grain and only begins to decrease when the twin volume fraction exceeds 35%. Thus, when the twin is still fine (<35% in volume fraction), the conditions are favorable for forming a second twin in the same grain. Next we apply the model to examine whether twin-DD interactions can affect the preference for achieving the same twin volume fraction by one or two twins.

In the model, as with the first twin, the second twin is formed where the stress concentrations are the highest along the region where the twin boundary intersects the grain boundary. Fig. 11 shows the von Mises contour maps for the two twin cases (configurations) for all three types of twin-DD interactions. We find that in this case, the tips of the bottom twin experience a different stress state than the upper twin tips. This can be expected since the two twins have different neighbors and morphologies. Fig. 12 shows the slip activity maps. Compared to similar maps for the single twin cases, we observe that having one versus two twins does not substantially affect the slip activity in the matrix (again predominantly basal slip) and in the twin (mixed mode slip of pyramidal, basal and prismatic). Once again, the type of twin-DD interactions has second-order effects on the slip activity in the two-twin cases.

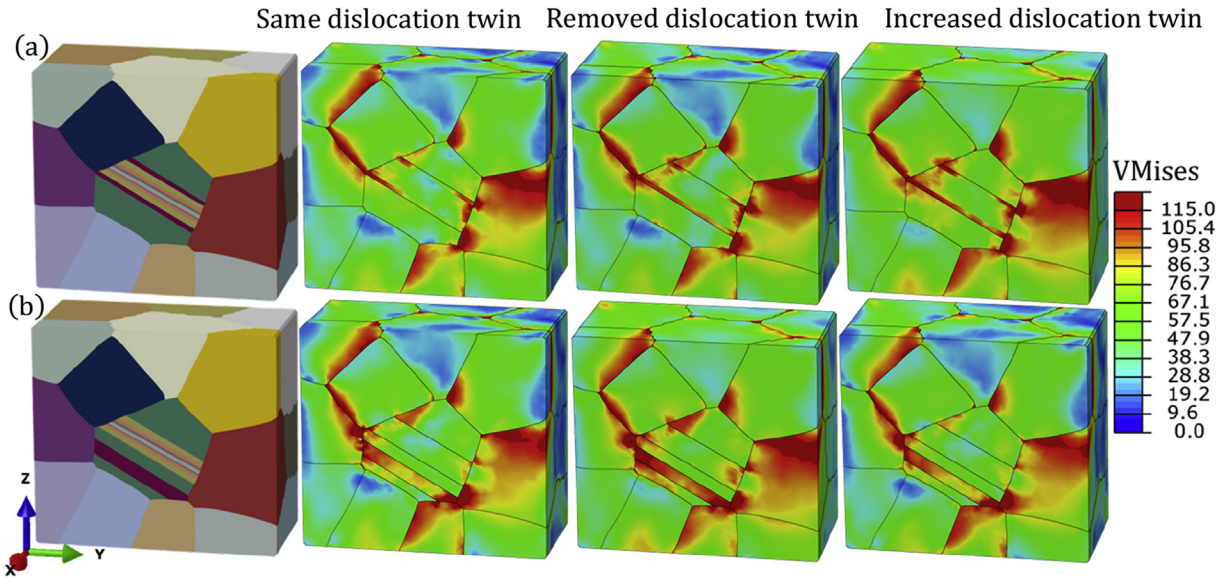

Fig. 11. Two grain structure configurations with parent grain containing (a) one 45% twin lamella and (b) two lamellae, one of 36% and another of 9% volume fraction. Distributions of the von Mises stress contours for all three types of twin-DD interactions are shown.

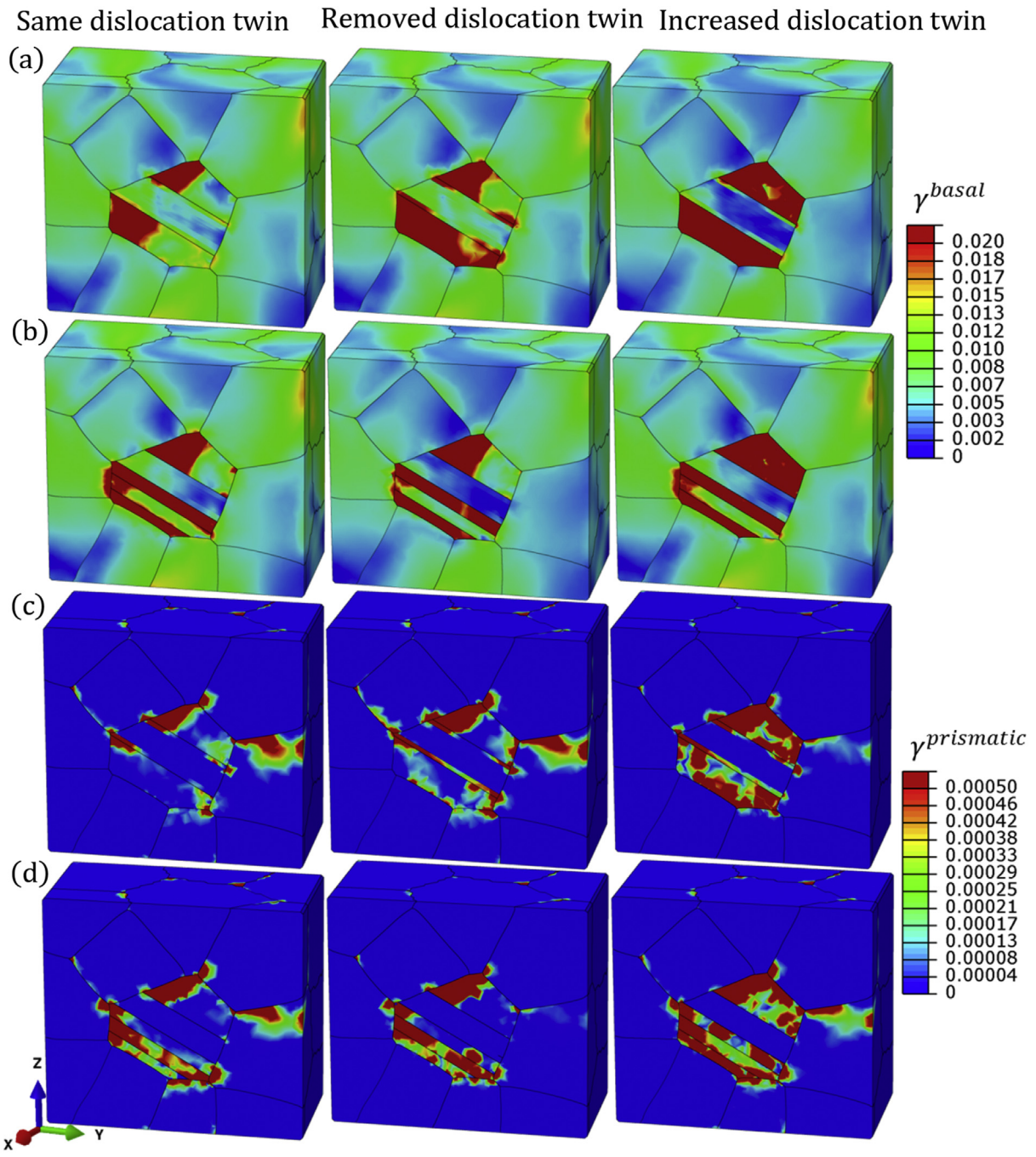

Fig. 12. Distributions of the accumulated shear strains across the whole grain model for basal and prismatic slip systems after equal amount of applied strain of approximately 0.005 with one and two lamellae grain configurations. Accumulated shear strains on basal slip mode in a grain model containing (a) one twin lamella, (b) two twin lamellae and prismatic slip mode with (c) one twin lamella and (d) two twin lamellae. The comparison is also made considering all three types of DD-twin interactions.

The calculation is carried out on both the one twin and the two-twin configurations needed to achieve 45% twin volume fraction. To determine whether one or two twins is more favorable, we incremented the applied plastic strain and calculated the associated increment in strain energy in four volumes: the parent, the twin lamellae, the entire grain (parent + twin), and the entire multi-grain cluster and considered changes in the plastic work W_s, where s represents the number of twin lamellae in the grain model. This change is calculated for the four domains using the relationship $W_s = \frac{1}{V}\sum_1^n \int_V \sigma_{ij} \Delta\varepsilon_{ij}^p$, where the increment in plastic strain of 0.005 is applied from the same *onset* configuration, i.e., the configuration after incrementing

Table 2
Comparison of plastic work difference between one lamella and two twin lamellae calculated over the specific volume as indicated in the table.

	Same dislocation twin	Removed dislocation twin	Increased dislocation twin
	$\Delta W \left[\frac{MJ}{m^3}\right] x10^4$	$\Delta W \left[\frac{MJ}{m^3}\right] x10^4$	$\Delta W \left[\frac{MJ}{m^3}\right] x10^4$
Grain cluster	0.28	−2.06	2.4
Parent grain + twin	0.29	−0.17	0.4
Parent grain	0.13	−0.12	0.03
Twin lamella	0.16	−0.05	0.37

either the existing lamella to 45% volume fraction for the one twin case or the configuration after creating the second lamellae without incrementing the existing lamella to 45% volume fraction for the two lamellae case. The results are then compared for each DD-twin interaction case and the difference between the two twin grain configurations is calculated as: $\Delta W = W_1 - W_2$ (Table 2). Table 2 presents calculations of the system energy when the 45% twin volume fraction is embodied in one lamella or two separate lamellae. These results show a remarkable effect of twin-DD interactions. When the stored density is maintained or increased, forming a second twin lamella (with 9% volume fraction) is more energetically favorable than increasing the volume fraction of the original lamella. Although not shown, the twin driving force in the parent grain along the two twin boundaries would lead to the same conclusion. It is just slightly higher in the case of two separate twin lamellae than in the one twin lamella case. However, when the twin removes dislocation density, growth of a single twin is preferred.

To better understand the preference, we analyzed the dislocation density evolution within the twin lamella and the parent matrix. Fig. 13 presents the calculated evolution of the dislocation density on each slip mode (a) within the parent matrix of the twinned grain and (b-d) within the twin lamellae for the three different cases. Despite the preference for basal slip in this

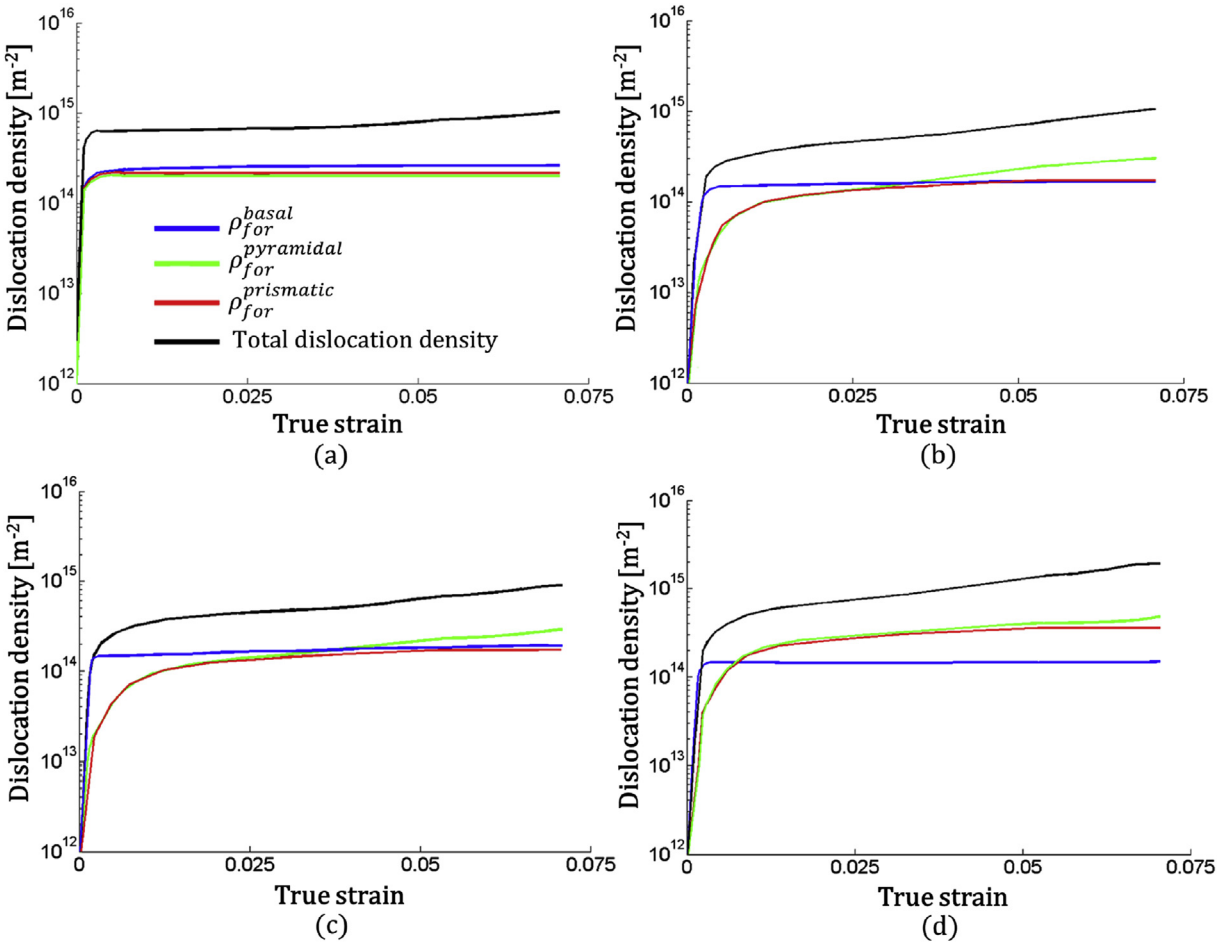

Fig. 13. Evolution of the dislocation density in (a) the parent matrix and (b–d) the twinned domains for three different dislocation density cases, (b) same dislocation twin, (c) removed dislocation twin, and (d) increased dislocation twin case. There was no significant difference in the dislocation storage rates for the parent matrix in the three cases so (a) is representative of the state of the parent matrix in all three cases. The total DD in (b–d) is the same as in Fig. 8.

alloy, all slip modes are active within the parent matrix and within the twin lamella. For the matrix, basal slip slightly dominates. The selected slip modes in the parent matrix are also not sensitive to how the growing twin affects the stored dislocations and thus it suffices to show the representative calculation in Fig. 13a. We found that the evolution of the dislocation densities in the parent matrix is similar for all three different DD-twin cases that were considered. This suggests that the parent orientation and that of its next nearest neighboring grains largely govern slip activity in the parent. The most interesting difference among the three cases within the twin lamella is that the removed dislocation twin case can be distinguished by a lower dislocation density than the parent and the lowest activity of pyramidal slip among the three cases. We propose that these differences provide an explanation for why self-thickening would be favored over formation of a new twin for the situation in which twin thickening recovers previously stored dislocations. It has recently been reported that dislocations can readily be transmitted through extension twins in Mg alloys (Molodov et al., 2017). As a result, extension twins in AZ31 could contain a low level of dislocation density. Since extension twins in AZ31 are observed to be thick with majority of grains containing a single or low multiplicity of twin lamellae (Knezevic et al., 2010), our results about the effect of low level of stored dislocations in twin domain on self-thickening is consistent with this new finding about the transmissivity.

5. Conclusions

Using the recently developed framework for explicitly modeling discrete twin lamellae within a 3D crystal plasticity finite element (CPFE) models, we investigated the effects of dislocation density on twin propagation. For a magnesium alloy AZ31 containing extension twins, we calculated the stress fields and analyzed the driving forces for twin growth for three cases of twin dislocation density: full recovery (the twin domain removes the stored dislocation density), maintenance (the twin domain retains it), and the Basinski effect (the twin domain adopts a much larger stored dislocation density, by two times in this case). We show that these cases have little effect on the twin growth rate, the stress field in the twin and neighboring grains, and the slip activity inside and outside the twin. However, we find that the increase in dislocation density content within the twinned region can slow down the twin propagation process and increase the rate of stored dislocations in the entire grain and thus its hardness. The analysis also suggests that when a twin recovers dislocations as it grows self-thickening is preferred over forming a second twin lamella. On the basis of the results here, we propose that this preference occurs when the rate of evolution of dislocation density within the twin is slower than that of the parent.

Acknowledgements

This work is based upon a project supported by the U.S. National Science Foundation (NSF) under grant no. CMMI-1650641. I. J. B. acknowledges financial support from NSF under grant no. CMMI-1728224. Additionally, M.A. wishes to acknowledge the support from the graduate school at the University of New Hampshire through Dissertation Year Fellowship program.

Appendix A

Here, we present for completeness a summary of a dislocation density hardening law formulation used to compute the evolution of slip and twin resistances as a function of strain, temperature and strain rate originally proposed in (Beyerlein and Tomé, 2008).

The resistance for activation of slip considers contributions of several different terms: a friction stress $\tau^{\alpha}_{0,f}$, a forest dislocation interaction stress τ^{α}_{for} and a dislocation substructure interaction stress τ^{α}_{sub}

$$\tau^{\alpha}_{c} = \tau^{\alpha}_{0,f} + \tau^{\alpha}_{for} + \tau^{\alpha}_{sub}. \tag{A1}$$

The model for the resistance for twin activation differs from that for slip. It accounts two distinct contributions: a temperature-independent friction term τ^{β}_{0} and a latent hardening term coupling the active slip and the twin systems. It is expressed as

$$\tau^{\beta}_{c} = \tau^{\beta}_{0} + \mu^{\beta} \sum_{\alpha} C^{\alpha\beta} b^{\beta} b^{\alpha} \rho^{\alpha}_{for}. \tag{A2}$$

Here μ^{β}, b^{β} and $C^{\alpha\beta}$ represent the elastic shear modulus, Burgers vector on the given twin system, and the latent hardening matrix used for coupling, respectively. The behavior of τ^{α}_{for} and τ^{α}_{sub} is governed by the evolution of the dislocation densities in the form of forest ρ^{α}_{for} and substructure ρ^{α}_{sub} dislocations. These relationships, for each dislocation type, can be expressed in the form of a Taylor law

$$\tau^{\alpha}_{for} = \chi b^{\alpha} \mu^{\alpha} \sqrt{\rho^{\alpha}_{for}}, \text{and, } \tau^{\alpha}_{sub} = k_{sub} \mu^{\alpha} b^{\alpha} \sqrt{\rho_{sub}} \log\left(\frac{1}{b^{\alpha}\sqrt{\rho_{sub}}}\right), \tag{A3}$$

where $\chi = 0.9$ is a dislocation interaction parameter and $k_{sub} = 0.086$ is a mathematical parameter that insures that Eq. (A3) compensates the Taylor law at low dislocation densities. Since the material is assumed to start in an annealed state, the initial

dislocation density in all simulations was set to 10^{12} m^{-2}. The stored forest density ρ^{α}_{for} evolves via a competition between the rate of storage and the rate of dynamic recovery:

$$\frac{\partial \rho^{\alpha}_{for}}{\partial \gamma^{\alpha}} = \frac{\partial \rho^{\alpha}_{gen,for}}{\partial \gamma^{\alpha}} - \frac{\partial \rho^{\alpha}_{rem,for}}{\partial \gamma^{\alpha}} = k^{\alpha}_{1}\sqrt{\rho^{\alpha}_{for}} - k^{\alpha}_{2}(\dot{\varepsilon}, \mathrm{T})\rho^{\alpha}_{for}, \qquad \Delta\rho^{\alpha}_{for} = \frac{\partial \rho^{\alpha}_{for}}{\partial \gamma^{\alpha}}|\Delta\gamma^{\alpha}|, \tag{A4}$$

where k^{α}_{1} is a coefficient for the rate of dislocation storage due to statistical trapping of gliding dislocations by the forest obstacles and k^{α}_{2} is the coefficient for the rate of dynamic recovery, which is given by the following expression:

$$\frac{k^{\alpha}_{2}(\dot{\varepsilon}, \mathrm{T})}{k^{\alpha}_{1}} = \frac{\chi b^{\alpha}}{g^{\alpha}}\left(1 - \frac{kT}{D^{\alpha}b^{3}} ln\left(\frac{\dot{\varepsilon}}{\dot{\varepsilon}_{0}}\right)\right). \tag{A5}$$

In Eq. (A5), k, $\dot{\varepsilon}_{0}$, g^{α} and D^{α} are respectively Boltzmann's constant, a reference strain rate, an effective activation enthalpy and a drag stress. Furthermore, the increment in substructure development is proportional to the rate of dynamic recovery of all active dislocations and can be expressed as:

$$\Delta\rho_{sub} = \sum_{\alpha} qb^{\alpha}\frac{\partial \rho^{\alpha}_{rem,for}}{\partial \gamma^{\alpha}}|\Delta\gamma^{\alpha}|, \tag{A6}$$

where q is a coefficient defining the fraction of an α-type dislocations that do not annihilate but become substructure dislocation. The hardening parameters have been calibrated in the earlier study and used here.

Appendix B

This appendix provides a more detailed description of the automated procedure developed for twin lamella incorporation into finite element (FE) mesh. The procedure provides explanation of the necessary steps to initially form a twin lamella in a previously selected parent grain, which can be further thickened with additional straining of the polycrystal (granular microstructure). Additional straining is conducted via a series of consecutive deformation steps resulting in an incremental increase of the twin's volume. These deformation steps are necessary, because straining has to be interrupted at specific strain levels to alter the FE mesh and reflect the twin formation and growth. The number of these deformation steps depends primarily on how often polycrystal deformation is interrupted and the amount of twin volume increment used to thicken/grow the twin lamella. In order to better facilitate description of this procedure Fig. B1 is shown. Next, the procedure performed between deformation steps to either initially form/propagate or thicken/grow a pre-existing twin lamella in selected parent grain is described.

As previously mentioned, this procedure is made autonomous thanks to scripting capabilities provided in Matlab, Patran and Abaqus software packages. A master script developed in Matlab was used to write appropriate Patran and Python script files with sets of specific commands necessary to be executed in Patran and Abaqus, respectively. Patran was mainly used to perform surface or solid meshing, while Abaqus was used to extract the surface mesh from the solid mesh model or to perform the Abaqus mesh cleanup procedure.

Once the deformation step is accomplished to a certain prescribed strain level (Fig. B1a), procedure starts by obtaining the deformed surface meshes of all individual grains (Fig B1b). This step in the procedure is always performed independently on whether a new twin lamella will be formed first or an existing twin lamella will be thicken for a prescribed volume increment. At this stage, the predominant twin system (*pts*) and its location have already been determined. Next, either forming (Fig. B1c) or thickening (Fig. B1d) of a twin lamella is performed. Knowing the predominant twin system in the parent grain, the two corresponding twin planes in 3D at specific distance where twin lamella is located in the parent grain can be defined. This distance should reflect the incremental growth of a twin lamella achieved in the previous deformation step. The Matlab script determines the intersection points between these two twin cutting planes and the 3D surface mesh of the parent grain. The Patran script then uses coordinates of these points to reconstruct the closed loops that define each of the two intersected planes and to mesh them with triangular elements. After the meshing is done, intersection plane surface meshes are exported, which are then used to construct a new parent and twin grain surface meshes. The new twin surface mesh determines the increment in twin's volume and for each deformation step they are all differently colored, as it is shown in Fig. 5 in the paper. Next, the Matlab script writes a Python script for surface mesh cleanup in Abaqus to collapse any elements with bad aspect ratio. This procedure is performed on a surface mesh of a whole polycrystal. Every triangular element with the edge aspect ratio greater than 4 is been collapsed. Finally, the Matlab script writes an Abaqus input file containing the new mesh, state variables, and boundary conditions for the subsequent deformation step.

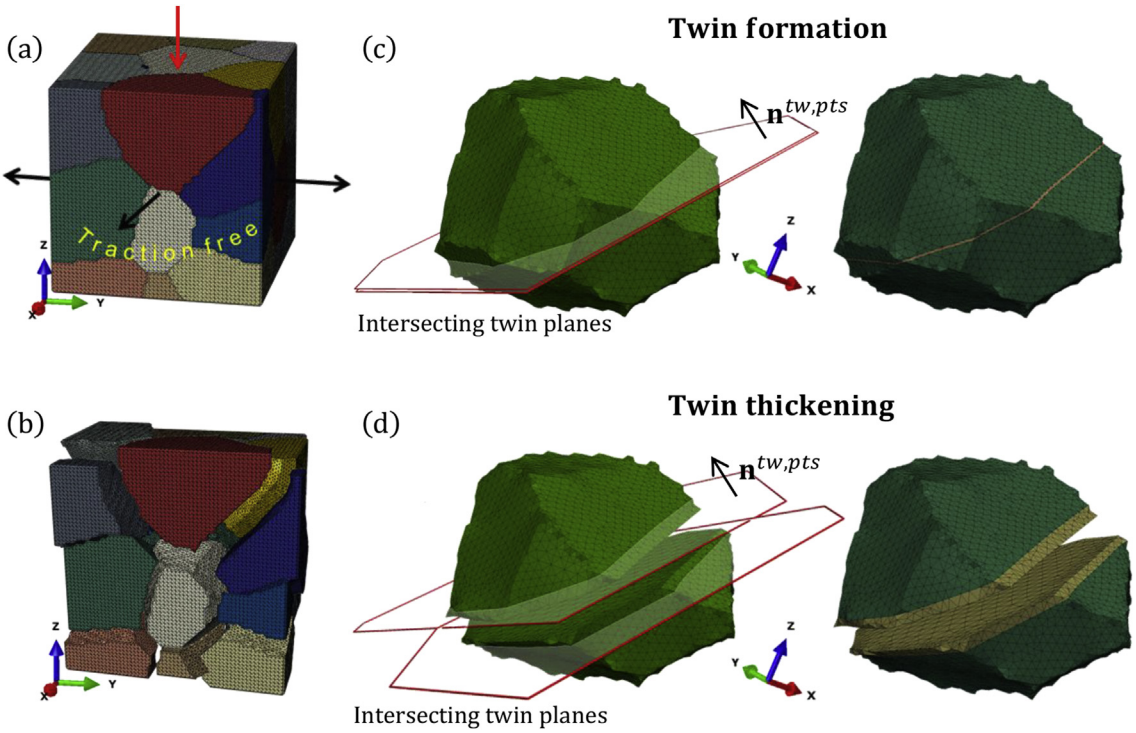

Fig. B1. Procedure for explicit incorporation of twinning in CPFE: (a) Deformation step performed in simple compression; (b) Individually deformed surface meshes of all grains. The intersection between the two twin cutting planes and the 3D surface mesh of the parent grain in the case of (c) twin formation and (d) twin thickening. Differently colored regions (on the right hand side images (c) and (d)) represent the surface mesh of the increment in twin volume.

Appendix C

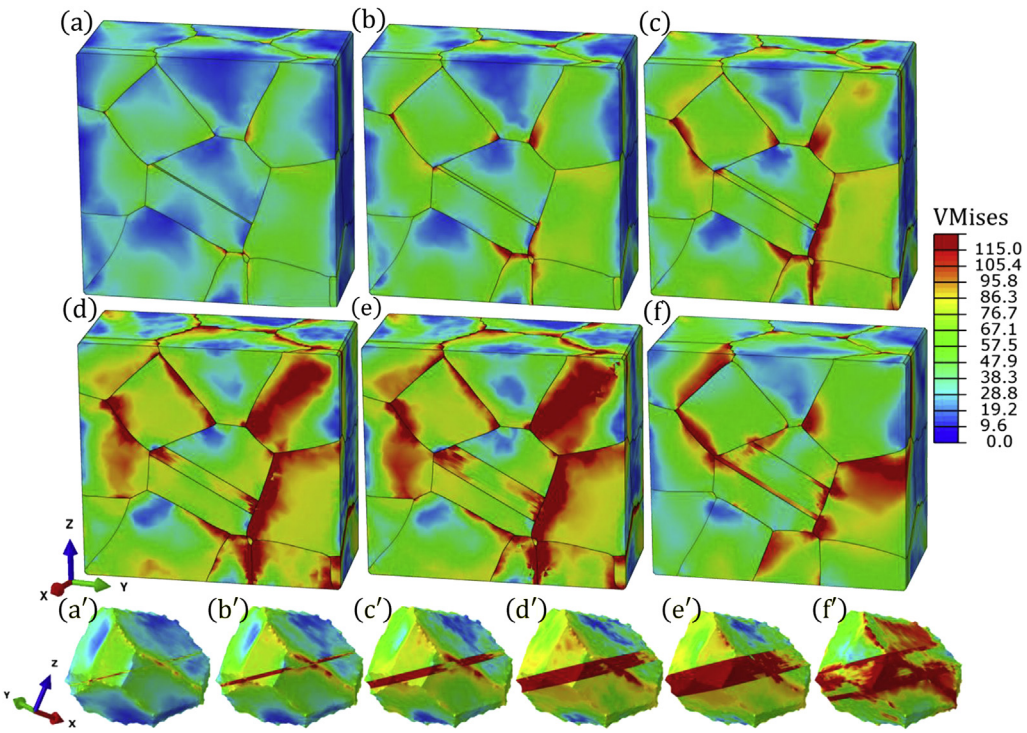

Fig. C1. Distributions of the von Mises stress (VMises) for different twin volume fractions (removed dislocation twin i.e. case 2): (a and a') 2% twin, (b and b') 5% twin, (c and c') 10% twin, (d and d') 20% twin, (e and e') 36% twin and (f and f') 45% twin. In the bottom row (denoted with primed labels) the corresponding parent and twin grains pulled out from the rest of the grains in the cluster are shown.

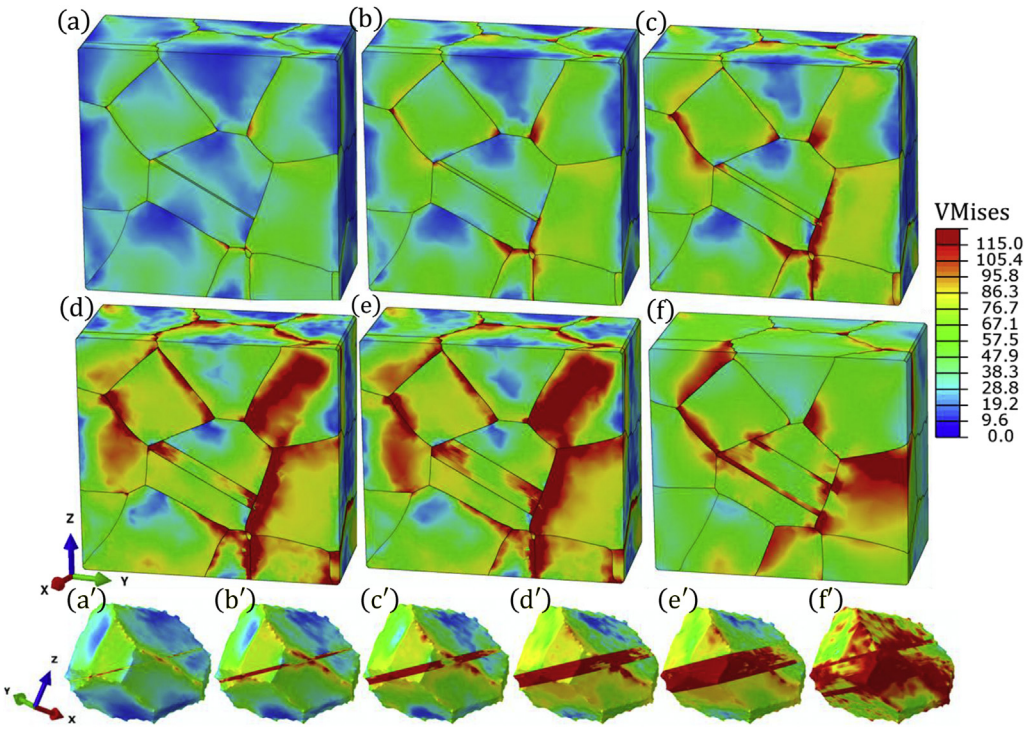

Fig. C2. Distributions of the von Mises stress (VMises) for different twin volume fractions (increased dislocation twin i.e. case 3): (a and a') 2% twin, (b and b') 5% twin, (c and c') 10% twin, (d and d') 20% twin, (e and e') 36% twin and (f and f') 45% twin. In the bottom row (denoted with primed labels) the corresponding parent and twin grains pulled out from the rest of the grains in the cluster are shown.

Appendix D. Supplementary data

Supplementary data related to this article can be found at http://dx.doi.org/10.1016/j.ijplas.2017.09.002.

References

Ardeljan, M., Beyerlein, I.J., Knezevic, M., 2014. A dislocation density based crystal plasticity finite element model: application to a two-phase polycrystalline HCP/BCC composites. J. Mech. Phys. Solids 66, 16–31.
Ardeljan, M., Knezevic, M., Nizolek, T., Beyerlein, I.J., Mara, N.A., Pollock, T.M., 2015a. A study of microstructure-driven strain localizations in two-phase polycrystalline HCP/BCC composites using a multi-scale model. Int. J. Plast. 74, 35–57.
Ardeljan, M., McCabe, R.J., Beyerlein, I.J., Knezevic, M., 2015b. Explicit incorporation of deformation twins into crystal plasticity finite element models. Comput. Methods Appl. Mech. Eng. 295, 396–413.
Ardeljan, M., Beyerlein, I.J., McWilliams, B.A., Knezevic, M., 2016. Strain rate and temperature sensitive multi-level crystal plasticity model for large plastic deformation behavior: application to AZ31 magnesium alloy. Int. J. Plast. 83, 90–109.
Arul Kumar, M., Beyerlein, I.J., Tomé, C.N., 2016. Effect of local stress fields on twin characteristics in HCP metals. Acta Mater. 116, 143–154.
Asaro, R.J., Needleman, A., 1985. Texture development and strain hardening in rate dependent polycrystals. Acta Metall. Mater 33, 923–953.
Aydıner, C.C., Bernier, J.V., Clausen, B., Lienert, U., Tomé, C.N., Brown, D.W., 2009. Evolution of stress in individual grains and twins in a magnesium alloy aggregate. Phys. Rev. B 80, 024113.
Basinski, Z.S., Basinski, S.J., 1989. Copper single crystal PSB morphology between 4.2 and 350 K. Acta Metall. 37, 3263–3273.
Basinski, Z.S., Szczerba, M.S., Niewczas, M., Embury, J.D., Basinski, S.J., 1997. Transformation of slip dislocations during twinning of copper-aluminum alloy crystals. Revue de Metallurgie. Cah. D'Informations Tech. 94, 1037–1044.
Bathe, K.-J., 1996. Finite Element Procedures. Prentice Hall, Englewood Cliffs, N.J.
Bell, R.L., Cahn, R., 1957. The dynamics of twinning and the interrelation of slip and twinning in zinc crystals. Proceedings of the Royal Society of London. Ser. A. Math. Phys. Sci. 239, 494–521.
Beyerlein, I.J., Tomé, C.N., 2008. A dislocation-based constitutive law for pure Zr including temperature effects. Int. J. Plast. 24, 867–895.
Beyerlein, I.J., McCabe, R.J., Tomé, C.N., 2011. Effect of microstructure on the nucleation of deformation twins in polycrystalline high-purity magnesium: a multi-scale modeling study. J. Mech. Phys. Solids 59, 988–1003.
Beyerlein, I.J., Zhang, X., Misra, A., 2014. Growth twins and deformation twins in metals. Annu. Rev. Mater. Res. 44, 329–363.
Bieler, T.R., Wang, L., Beaudoin, A.J., Kenesei, P., Lienert, U., 2014. In situ characterization of twin nucleation in pure Ti using 3d-XRD. Metallurgical Mater. Trans. A 45, 109–122.
Capolungo, L., Beyerlein, I.J., 2008. Nucleation and stability of twins in hcp metals. Phys. Rev. B 78024117.
Capolungo, L., Beyerlein, I.J., Kaschner, G.C., Tomé, C.N., 2009. On the interaction between slip dislocations and twins in HCP. Zr. Mater. Sci. Eng. A 513–514, 42–51.
Cheng, J., Ghosh, S., 2015. A crystal plasticity FE model for deformation with twin nucleation in magnesium alloys. Int. J. Plast. 67, 148–170.
Cheng, J., Ghosh, S., 2017. Crystal plasticity finite element modeling of discrete twin evolution in polycrystalline magnesium. J. Mech. Phys. Solids 99, 512–538.
Christian, J.W., Mahajan, S., 1995. Deformation twinning. Prog. Mater. Sci. 39, 1–157.

El Kadiri, H., Oppedal, A.L., 2010. A crystal plasticity theory for latent hardening by glide twinning through dislocation transmutation and twin accommodation effects. J. Mech. Phys. Solids 58, 613–624.
Fromm, B.S., Adams, B.L., Ahmadi, S., Knezevic, M., 2009. Grain size and orientation distributions: application to yielding of α-titanium. Acta. Mater 57, 2339–2348.
Groeber, M.A., Jackson, M.A., 2014. DREAM. 3D: a digital representation environment for the analysis of microstructure in 3D. Integrating Mater. Manuf. Innovation 3, 5.
Groeber, M., Ghosh, S., Uchic, M.D., Dimiduk, D.M., 2008. A framework for automated analysis and simulation of 3D polycrystalline microstructures. Part 2: synthetic structure generation. Acta. Mater 56, 1274–1287.
Hutchinson, J.W., 1976. Bounds and self-consistent estimates for creep of polycrystalline materials. Proceedings of the Royal Society of London. Ser. A, Math. Phys. Sci. 348, 101–126.
Jahedi, M., McWilliams, B.A., Moy, P., Knezevic, M., 2017. Deformation twinning in rolled WE43-T5 rare earth magnesium alloy: influence on strain hardening and texture evolution. Acta. Mater 131, 221–232.
Kalidindi, S.R., 1998. Incorporation of deformation twinning in crystal plasticity models. J. Mech. Phys. Solids 46, 267–271.
Kalidindi, S.R., Bronkhorst, C.A., Anand, L., 1992. Crystallographic texture evolution in bulk deformation processing of FCC metals. J. Mech. Phys. Solids 40, 537–569.
Kalidindi, S.R., Duvvuru, H.K., Knezevic, M., 2006. Spectral calibration of crystal plasticity models. Acta. Mater 54, 1795–1804.
Kaschner, G.C., Tomé, C.N., Beyerlein, I.J., Vogel, S.C., Brown, D.W., McCabe, R.J., 2006. Role of twinning in the hardening response of zirconium during temperature reloads. Acta. Mater 54, 2887–2896.
Knezevic, M., Landry, N.W., 2015. Procedures for reducing large datasets of crystal orientations using generalized spherical harmonics. Mech. Mater. 88, 73–86.
Knezevic, M., Levinson, A., Harris, R., Mishra, R.K., Doherty, R.D., Kalidindi, S.R., 2010. Deformation twinning in AZ31: influence on strain hardening and texture evolution. Acta. Mater 58, 6230–6242.
Knezevic, M., Capolungo, L., Tomé, C.N., Lebensohn, R.A., Alexander, D.J., Mihaila, B., McCabe, R.J., 2012. Anisotropic stress-strain response and microstructure evolution of textured α-uranium. Acta. Mater 60, 702–715.
Knezevic, M., Beyerlein, I.J., Brown, D.W., Sisneros, T.A., Tomé, C.N., 2013a. A polycrystal plasticity model for predicting mechanical response and texture evolution during strain-path changes: application to beryllium. Int. J. Plast. 49, 185–198.
Knezevic, M., Lebensohn, R.A., Cazacu, O., Revil-Baudard, B., Proust, G., Vogel, S.C., Nixon, M.E., 2013b. Modeling bending of α-titanium with embedded polycrystal plasticity in implicit finite elements. Mater. Sci. Eng. A 564, 116–126.
Knezevic, M., McCabe, R.J., Lebensohn, R.A., Tomé, C.N., Liu, C., Lovato, M.L., Mihaila, B., 2013c. Integration of self-consistent polycrystal plasticity with dislocation density based hardening laws within an implicit finite element framework: application to low-symmetry metals. J. Mech. Phys. Solids 61, 2034–2046.
Knezevic, M., McCabe, R.J., Tomé, C.N., Lebensohn, R.A., Chen, S.R., Cady, C.M., Gray Iii, G.T., Mihaila, B., 2013d. Modeling mechanical response and texture evolution of α-uranium as a function of strain rate and temperature using polycrystal plasticity. Int. J. Plast. 43, 70–84.
Knezevic, M., Beyerlein, I.J., Lovato, M.L., Tomé, C.N., Richards, A.W., McCabe, R.J., 2014a. A strain-rate and temperature dependent constitutive model for BCC metals incorporating non-Schmid effects: application to tantalum–tungsten alloys. Int. J. Plast. 62, 93–104.
Knezevic, M., Carpenter, J.S., Lovato, M.L., McCabe, R.J., 2014b. Deformation behavior of the cobalt-based superalloy Haynes 25: experimental characterization and crystal plasticity modeling. Acta. Mater 63, 162–168.
Knezevic, M., Drach, B., Ardeljan, M., Beyerlein, I.J., 2014c. Three dimensional predictions of grain scale plasticity and grain boundaries using crystal plasticity finite element models. Comput. Methods Appl. Mech. Eng. 277, 239–259.
Knezevic, M., Jahedi, M., Korkolis, Y.P., Beyerlein, I.J., 2014d. Material-based design of the extrusion of bimetallic tubes. Comput. Mater. Sci. 95, 63–73.
Knezevic, M., Zecevic, M., Beyerlein, I.J., Bhattacharyya, A., McCabe, R.J., 2015a. Predicting texture evolution in Ta and Ta-10W alloys using polycrystal plasticity. JOM 67, 2670–2674.
Knezevic, M., Zecevic, M., Beyerlein, I.J., Bingert, J.F., McCabe, R.J., 2015b. Strain rate and temperature effects on the selection of primary and secondary slip and twinning systems in HCP Zr. Acta Mater. 88, 55–73.
Knezevic, M., Crapps, J., Beyerlein, I.J., Coughlin, D.R., Clarke, K.D., McCabe, R.J., 2016a. Anisotropic modeling of structural components using embedded crystal plasticity constructive laws within finite elements. Int. J. Mech. Sci. 105, 227–238.
Knezevic, M., Daymond, M.R., Beyerlein, I.J., 2016b. Modeling discrete twin lamellae in a microstructural framework. Scr. Mater 121, 84–88.
Kumar, A.M., Kanjarla, A.K., Niezgoda, S.R., Lebensohn, R.A., Tomé, C.N., 2015. Numerical study of the stress state of a deformation twin in magnesium. Acta. Mater 84, 349–358.
Landry, N., Knezevic, M., 2015. Delineation of first-order elastic property closures for hexagonal metals using fast fourier transforms. Materials 8, 6326–6345.
Lentz, M., Klaus, M., Beyerlein, I.J., Zecevic, M., Reimers, W., Knezevic, M., 2015a. In situ X-ray diffraction and crystal plasticity modeling of the deformation behavior of extruded Mg–Li–(Al) alloys: an uncommon tension–compression asymmetry. Acta. Mater 86, 254–268.
Lentz, M., Klaus, M., Wagner, M., Fahrenson, C., Beyerlein, I.J., Zecevic, M., Reimers, W., Knezevic, M., 2015b. Effect of age hardening on the deformation behavior of an Mg–Y–Nd alloy: in-situ X-ray diffraction and crystal plasticity modeling. Mater. Sci. Eng. A 628, 396–409.
Mahajan, S., 2013. Critique of mechanisms of formation of deformation, annealing and growth twins: face-centered cubic metals and alloys. Scr. Mater. 68, 95–99.
Mendelson, S., 1969. Zonal dislocations and twin lamellae in h.c.p. metals. Mater. Sci. Eng. 4, 231–242.
Mendelson, S., 1970. Zonal dislocations and dislocation reactions with twins in HCP metals. Scr. Metall. 4, 5–8.
Molnár, P., Jäger, A., Lejček, P., 2012. Twin nucleation at grain boundaries in Mg–3wt.% Al–1wt.% Zn alloy processed by equal channel angular pressing. Scr. Mater 67, 467–470.
Molodov, K.D., Al-Samman, T., Molodov, D.A., 2017. Profuse slip transmission across twin boundaries in magnesium. Acta. Mater 124, 397–409.
Niewczas, M., 2010. Lattice correspondence during twinning in hexagonal close-packed crystals. Acta. Mater 58, 5848–5857.
Patran, 2013. MSC Software Corporation (Newport Beach, CA, USA).
Risse, M., Lentz, M., Fahrenson, C., Reimers, W., Knezevic, M., Beyerlein, I.J., 2017. Elevated temperature effects on the plastic anisotropy of an extruded Mg-4 Wt Pct Li alloy: experiments and polycrystal modeling. Metall. Mater. Trans. A 48, 446–458.
Salem, A.A., Kalidindi, S.R., Doherty, R.D., 2003. Strain hardening of titanium: role of deformation twinning. Acta. Mater 51, 4225–4237.
Salem, A.A., Kalidindi, S.R., Doherty, R.D., Semiatin, S.L., 2006. Strain hardening due to deformation twinning in α-titanium: Mechanisms. Metallurgical Mater. Trans. A 37, 259–268.
Savage, D.J., Beyerlein, I.J., Knezevic, M., 2017a. Coupled texture and non-Schmid effects on yield surfaces of body-centered cubic polycrystals predicted by a crystal plasticity finite element approach. Int. J. Solids Struct. 109, 22–32.
Savage, D.J., Cazacu, O., Knezevic, M., 2017b. Dilational response of voided polycrystals. JOM 69, 942–947.
Van Houtte, P., 1978. Simulation of the rolling and shear texture of brass by the Taylor theory adapted for mechanical twinning. Acta Metall. Mater 26, 591–604.
Wang, J., Beyerlein, I.J., Tomé, C.N., 2010a. An atomic and probabilistic perspective on twin nucleation in Mg. Scr. Mater 63, 741–746.
Wang, L., Eisenlohr, P., Yang, Y., Bieler, T.R., Crimp, M.A., 2010b. Nucleation of paired twins at grain boundaries in titanium. Scr. Mater 63, 827–830.
Wang, L., Yang, Y., Eisenlohr, P., Bieler, T., Crimp, M., Mason, D., 2010c. Twin nucleation by slip transfer across grain boundaries in commercial purity titanium. Metall. Mater. Trans. A 41, 421–430.

Wang, J., Beyerlein, I., Tomé, C., 2014. Reactions of lattice dislocations with grain boundaries in Mg: implications on the micro scale from atomic-scale calculations. Int. J. Plast. 56, 156–172.
Wu, X., Proust, G., Knezevic, M., Kalidindi, S.R., 2007. Elastic-plastic property closures for hexagonal close-packed polycrystalline metals using first-order bounding theories. Acta. Mater 55, 2729–2737.
Zecevic, M., Knezevic, M., 2015. A dislocation density based elasto-plastic self-consistent model for the prediction of cyclic deformation: application to Al6022-T4. Int. J. Plast. 72, 200–217.
Zecevic, M., Knezevic, M., 2017. Modeling of sheet metal forming based on implicit embedding of the elasto-plastic self-consistent formulation in shell elements: application to cup drawing of AA6022-T4. JOM 69, 922–929.
Zecevic, M., Knezevic, M., Beyerlein, I.J., Tomé, C.N., 2015a. An elasto-plastic self-consistent model with hardening based on dislocation density, twinning and de-twinning: application to strain path changes in HCP metals. Mater. Sci. Eng. A 638, 262–274.
Zecevic, M., McCabe, R.J., Knezevic, M., 2015b. A new implementation of the spectral crystal plasticity framework in implicit finite elements. Mech. Mater. 84, 114–126.
Zecevic, M., McCabe, R.J., Knezevic, M., 2015c. Spectral database solutions to elasto-viscoplasticity within finite elements: application to a cobalt-based FCC superalloy. Int. J. Plast. 70, 151–165.
Zecevic, M., Beyerlein, I.J., McCabe, R.J., McWilliams, B.A., Knezevic, M., 2016a. Transitioning rate sensitivities across multiple length scales: microstructure-property relationships in the Taylor cylinder impact test on zirconium. Int. J. Plast. 84, 138–159.
Zecevic, M., Knezevic, M., Beyerlein, I.J., McCabe, R.J., 2016b. Origin of texture development in orthorhombic uranium. Mater. Sci. Eng. A 665, 108–124.
Zecevic, M., Knezevic, M., Beyerlein, I.J., McCabe, R.J., 2016c. Texture formation in orthorhombic alpha-uranium under simple compression and rolling to high strains. J. Nucl. Mater. 473, 143–156.
Zecevic, M., Korkolis, Y.P., Kuwabara, T., Knezevic, M., 2016d. Dual-phase steel sheets under cyclic tension–compression to large strains: experiments and crystal plasticity modeling. J. Mech. Phys. Solids 96, 65–87.
Zecevic, M., Beyerlein, I.J., Knezevic, M., 2017. Coupling elasto-plastic self-consistent crystal plasticity and implicit finite elements: applications to compression, cyclic tension-compression, and bending to large strains. Int. J. Plast. 93, 187–211.
Zhang, R.Y., Daymond, M.R., Holt, R.A., 2008. A finite element model of deformation twinning in zirconium. Mater. Sci. Eng. A 473, 139–146.
Zheng, S.J., Beyerlein, I.J., Wang, J., Carpenter, J.S., Han, W.Z., Mara, N.A., 2012. Deformation twinning mechanisms from bimetal interfaces as revealed by in situ straining in the TEM. Acta. Mater 60, 5858–5866.